Master's thesis
Theoretical physics

SYK and SYK-like Models

Pyry Kuusela

May 20, 2017

Tutor: Esko Keski-Vakkuri

Censors: Esko Keski-Vakkuri
Kari Rummukainen

UNIVERSITY OF HELSINKI
Department of Physics

PL 64 (Gustaf Hällströmin katu 2)
00014 Helsingin yliopisto

HELSINGIN YLIOPISTO — HELSINGFORS UNIVERSITET — UNIVERSITY OF HELSINKI

Tiedekunta — Fakultet — Faculty	Laitos — Institution — Department
Faculty of Science	Department of Physics

Tekijä — Författare — Author
Pyry Kuusela

Työn nimi — Arbetets titel — Title

SYK and SYK-like Models

Oppiaine — Läroämne — Subject
Theoretical physics

Työn laji — Arbetets art — Level	Aika — Datum — Month and year	Sivumäärä — Sidoantal — Number of pages
Master's thesis	May 20, 2017	77 pages

Tiivistelmä — Referat — Abstract

In this thesis, we discuss the Sachdev-Ye-Kitaev (SYK) model and tensor models with similar properties. The SYK model is a quantum field theoretical model describing N interacting fermions, whose coupling constants are drawn from a Gaussian ensemble. Noteworthy properties of the SYK model include that it is analytically solvable in the large N limit, that it exhibits conformal symmetry at low energies and that it is maximally chaotic. These properties are remarkably similar to those of a $1+1$ dimensional Schwarzschild black hole. It has been conjectured the SYK model is a holographic dual to the black hole.

We introduce a set of Feynman rules for the SYK model. Using these rules, we show that in the large N limit the diagrams that contribute to the two-point function are all so-called iterated melonic diagrams. This allows us to derive a Schwinger-Dyson equation for the two-point function, which, in turn, can be solved exactly in the infrared limit.

We also consider the four-point function. In the large N limit, the leading-order correction to the four-point function is given by so-called ladder diagrams. This allows us to derive an explicit expression for the four-point function.

The SYK model can be generalized in a few different ways. In this thesis, we consider the generalization where the fermions act through q-fold interactions instead of quartic interactions present in the original SYK model. In particular, considerable simplifications can be achieved in the $q \to \infty$ limit or $q = 2$ case, which we study.

While the SYK model has many interesting properties, its random couplings limit its usability especially as a dual to a Schwarzschild black hole. We therefore also consider tensor models which do not have this drawback but manage to preserve the interesting properties of the SYK model.

In the last chapter, we briefly inspect the chaotic behaviour of the SYK and tensor models and derive Lyapunov exponent for them. It can be shown that the expression saturates an upper bound for Lyapunov exponents of a large class of quantum systems, including large N systems.

Avainsanat — Nyckelord — Keywords
SYK, Tensor models

Säilytyspaikka — Förvaringsställe — Where deposited

Muita tietoja — övriga uppgifter — Additional information

Contents

1. Introduction

The Sachdev-Ye-Kitaev (SYK) model is a quantum field theoretical model that describes N fermions in $0+1$ spacetime dimensions interacting through quartic interactions with randomised couplings drawn from a Gaussian ensemble. The SYK model is a variant of the Sachdev-Ye (SY) model, a random quantum spin system originally introduced to describe a Heisenberg magnet with random infinite-range interactions [1]. The SYK variant of the model was first introduced by Kitaev, who also proposed the model as a holographic dual to a black hole in the anti-de Sitter (AdS) spacetime [2].

The original SY model [1] is given by the Hamiltonian

$$H = \frac{1}{\sqrt{M}} \sum_{j,k=1}^{N} J_{j,k} \mathbf{S}_j \cdot \mathbf{S}_k, \tag{1.0.1}$$

where the couplings $J_{i,j}$ independent random variables drawn from a Gaussian distribution, each with the same variance and a mean of zero. The spins $\mathbf{S}_i$ are in some representation of $SU(M)$ [3]. The model becomes solvable in the limit where $N \to \infty$ and $M \to \infty$.

The SY model was first discussed in connection with holographic correspondence in [4], where Sachdev shows a close correspondence between holographic metals and the fractionalised Fermi liquid phase of the lattice Anderson model using the SY model to describe the fractionalized Fermi liquid.

Kitaev has proposed a variant of the SY model, called SYK model, with Majorana fermions in $0+1$ dimensional spacetime interacting through quartic interactions

whose couplings are again independent Gaussian random variables. The model has the following Hamiltonian:

$$H = \frac{1}{4!} \sum_{i,j,k,l=1}^{N} J_{i,j,k,l} \chi_i \chi_j \chi_k \chi_l. \tag{1.0.2}$$

The SYK model becomes solvable in the $N \to \infty$ limit, where the Feynman diagrams consist of so-called iterated melonic diagrams for the vacuum and the two-point diagrams and of so-called ladder diagrams for the four-point diagrams. This makes is possible to derive relatively simple expressions for the Schwinger-Dyson equations of the two-point and the four-point functions.

At low energies, the two-point functions are analytically solvable from the Schwinger-Dyson equations and exhibit conformal symmetry, which, however, is broken at higher energies. The conformal symmetry and its breaking at higher energies is also seen with the four-point functions.

By considering an out-of-time-order four-point function, we can calculate the Lyapunov exponent for the SYK model quantifying its chaotic behaviour. Doing this, we find that the SYK model at a finite temperature T has a Lyapunov exponent of $\lambda_L = 2\pi T$. It can be shown that this is the maximal allowed Lyapunov exponent for a large number of quantum systems, such as the large N systems of which the SYK model is an example [5]. The same bound is saturated by a black hole in Einstein gravity [6]. The maximally chaotic behaviour is particularly interesting when combined with the exact solvability since for classical systems the two properties are mutually exclusive [3].

Based on these properties and the similarities between the two- and four-point functions of a $1+1$ dimensional Schwarzschild black hole[1] and those of the SYK model, Kitaev has proposed this model as a holographic dual of a Schwarzschild black hole in $1+1$ dimensional spacetime that is asymptotically AdS [2].

[1] In $1+1$ dimensions there is not really Einstein theory of gravity. Here we say that quantities are calculated from a Schwarzshild black hole when we mean quantities calculated from a metric $ds^2 = -\frac{r(r-a)}{R^2}dt^2 + \frac{R^2}{r(r-a)}$ with R and a constant.

The proposed duality between the SYK model and black holes is an example of a more general AdS/CFT correspondence, a conjectured duality between strongly coupled gauge theories and gravitational theories on the AdS spacetime. The conjecture was introduced in the influential paper "The Large N Limit of Superconformal field theories and supergravity" by Maldacena [7]. The AdS/CFT correspondence claims that the generating functionals of the strongly coupled gauge theories and gravitational theories on the AdS spacetime are equal [8]. Although the AdS/CFT correspondence has not been proven rigorously, it has passed many tests and no counterexamples have been found. The correspondence allows the studying of strongly coupled gauge theories by considering weakly-coupled gravitational theories on the AdS spacetime and vice versa. This is useful because the perturbative methods do not work with strongly-coupled systems due to the lack of a small expansion parameter.

As a tool of investigating black holes, the SYK model has a few problems. One of the problems is that real quantum systems do not have random interactions that are then averaged over a probability distribution unlike the SYK model. Therefore it is not immediately clear if the SYK model can be used to investigate subtler properties of black holes [9]. More recently, Witten [9], building on the work of Gurau and collaborators [10, 11, 12], has proposed a new SYK-like tensor model which has many of the important properties of the SYK model, such as the same two and four-point functions in the large N limit. Unlike the SYK model, the tensor model does not have a drawback of random interactions.

In this Master's thesis, we first study the SYK model and its properties. We prove the important property that in the $N \to \infty$ limit the only diagrams that contribute to the two- or four-point functions are iterated melonic or ladder diagrams, respectively. Using this knowledge, we derive the Schwinger-Dyson equations for the two- and four-point functions and use them to find the functions in the infrared, or low-energy, limit, where the model has a conformal symmetry. Then we briefly consider

a natural generalization of the SYK model where, instead of quartic interactions, the fermions interact through q-fold interactions with arbitrary q. We find that in the limit $q \to \infty$ we get remarkably simple expressions for both two- and four-point functions. In the case of the two-point function, we also calculate the leading-order correction in the $q \to \infty$ limit.

After studying the SYK model, we turn to the tensor model proposed by Witten. For simplicity, we will restrict ourselves to a specific special case of the general type of the model Witten proposed, but the generalization to the general case should be obvious. We show that, as was the case with the SYK model, in the $N \to \infty$ limit the only diagrams that contribute to the two- and four-point functions are the iterated melonic and ladder diagrams, respectively. Then we show that this leads to essentially the same two- and four-point functions as for the SYK model. This shows that the models share the same important properties we have described above.

Finally, we investigate the chaotic behaviour of the SYK model. We begin by briefly describing how the chaotic behaviour can be quantified in quantum systems and then show that the SYK model has a maximal Lyapunov exponent $\lambda_L = 2\pi T$, which is a yet another property it shares with a black holes.

2. SYK Model

2.1 Introduction

The Sachdev-Ye-Kitaev model (SYK model) [1, 2] is a quantum field theoretical model with random quartic interaction between fermions in $0+1$ dimensions. The Hamiltonian of the SYK model for N fermions with 4-fold interactions is [2]

$$H = \frac{1}{4!}\sum_{i,j,k,l=1}^{N} J_{i,j,k,l}\chi_i\chi_j\chi_k\chi_l = \sum_{i\leq j\leq k\leq l} J_{i,j,k,l}\chi_i\chi_j\chi_k\chi_l, \tag{2.1.1}$$

which arises from the action:

$$S = \int dt \left(\sum_i \chi_i \frac{d}{dt}\chi_i + \frac{1}{4!}\sum_{i,j,k,l=1}^{N} J_{i,j,k,l}\chi_i\chi_j\chi_k\chi_l\right), \tag{2.1.2}$$

where χ_n are Majorana fermions so that $\{\chi_n, \chi_m\} = \delta_{mn}$. The coupling constants $J_{i,j,k,l}$ with different i, j, k, l are independent Gaussian random variables, each with the same average and variance. The only exception is that in order to account correctly for the anticommutation relations of the fermions, we must take $J_{i,j,k,l}$ to be antisymmetric for indices differing from each other, so that $J_{i,j,k,l} = -J_{j,i,k,l}$ when $i \neq j$, $J_{i,j,k,l} = -J_{i,k,j,l}$ when $j \neq k$, $J_{i,j,k,l} = -J_{k,j,i,l}$ when $i \neq k$ and so forth. Please note that this does not imply that $J_{i,j,k,l}$ is fully antisymmetric, since the antisymmetry is not required with respect to the exchange of two indices if both have the same value (see for example 2.1.4). We choose the Gaussian distribution so that the probability distribution of the coefficients $J_{i,j,k,l}$ is given by:

$$P(J_{i,j,k,l}) = C\exp\left(-\frac{N^3 J_{i,j,k,l}^2}{12J^2}\right), \tag{2.1.3}$$

where J is the same constant, which is related to the variance of the ensemble, for every $J_{i,j,k,l}$ and C is the normalization constant. Notice that the probability distribution is chosen so that it depends on the number of interacting fermions, N. This is necessary to get simple expressions for Feynman diagrams in the large N limit. For this probability distribution we have the following moments for the products of the couplings $J_{i,j,k,l}$, when we have used the antisymmetry of the couplings to set that $i \geq j \geq k \geq l$ and $m \geq n \geq o \geq p$:

$$\overline{J_{i,j,k,l}J_{m,n,o,p}} = \frac{3!J^2}{N^3}\delta_{im}\delta_{jn}\delta_{ko}\delta_{lp}, \qquad \overline{J_{i,j,k,l}} = 0. \tag{2.1.4}$$

When calculating explicit expressions for Feynman diagrams or correlation functions, taking the average over the Gaussian distribution (2.1.3) is always implied. This is also occasionally referred to as taking the average over the disorder.

2.2 Feynman Diagrams for the SYK Model

Feynman diagrams for the SYK theory consist of quadratic vertices with every vertex giving a factor of $J_{i,j,k,l}$. Since these couplings are drawn from a probability distribution, we must average over the probability distribution. Therefore the value of a vertex in a Feynman diagram depends on the couplings $J_{i,j,k,l}$. For example, averaging over $J^4_{0,0,0,0}$ and $J^2_{0,0,0,0}J^2_{1,0,0,0}$ gives different results:

$$\overline{J^4_{0,0,0,0}} = 3\left(\frac{3!J^2}{N^3}\right)^2, \qquad \overline{J^2_{0,0,0,0}J^2_{1,0,0,0}} = \left(\frac{3!J^2}{N^3}\right)^2. \tag{2.2.1}$$

To represent different combinations of coupling constants in Feynman diagrams, we can "break up" each vertex into four pieces and represent each different index with different colour. For example, denoting index i with colour blue j with red, k with green and l with yellow we get that the following vertex corresponds to the coupling constant $J_{i,j,k,l}$:

In the following we shall call the coloured dots *endpoints* and the coloured lines representing propagators *lines*. We can express the identities (2.1.4) in graphical form using coloured vertices as shown in the figures 2.2 and 2.3 (overline indicates

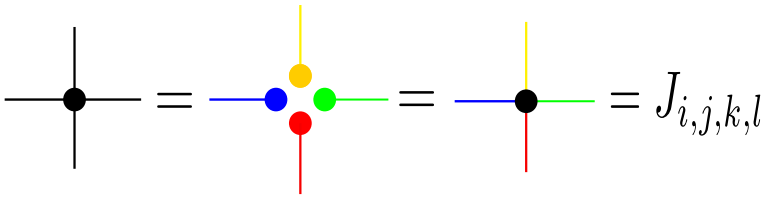

Figure 2.1: *Vertex giving a factor of $J_{i,j,k,l}$ presented in three equivalent ways.*

here the average over the Gaussian probability distribution):

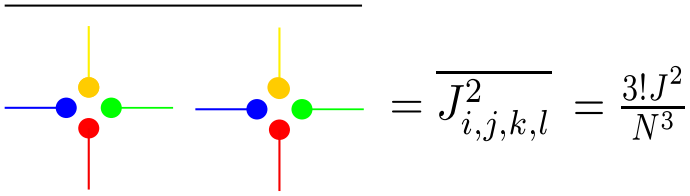

Figure 2.2: *A pair of vertices giving a factor of $\frac{3!J^2}{N^3}$ when averaged over the probability distribution.*

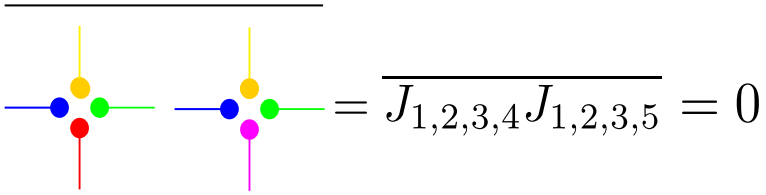

Figure 2.3: *Pair of vertices giving a factor of* 0 *when averaged over the probability distribution due to the two vertices having different indices (colours). Here blue represents index 1, yellow 2, green 3, red 4, and purple 5.*

Note that due to the antisymmetry properties of the coupling coefficients, a pair of vertices gives a nonzero contribution if the colours in one vertex can be permuted to match those of another vertex (see figure 2.4).

Since the contraction $\{\chi_i, \chi_j\}$ gives a factor of δ_{ij}, we see that the lines of one colour must always be connected to another line of the same colour. In addition, it follows from previous rules that there must be an even amount of vertices with the same colours in order for the coloured diagram to give a nonzero contribution. As an example, let us consider the figure 2.5, which shows a two-point diagram

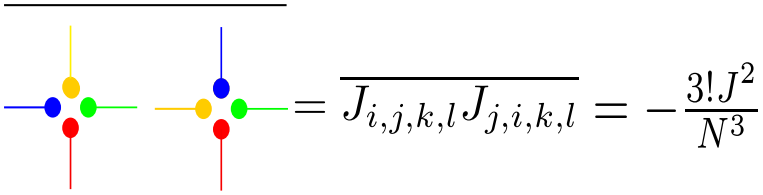

Figure 2.4: *Despite the vertices having different colours in corresponding endpoints, this pair of vertices gives a nonzero contribution when averaged over the probability distribution since the colours in the second vertex can be permuted to match those in the first one. The minus sign is due to the odd parity of the permutation.*

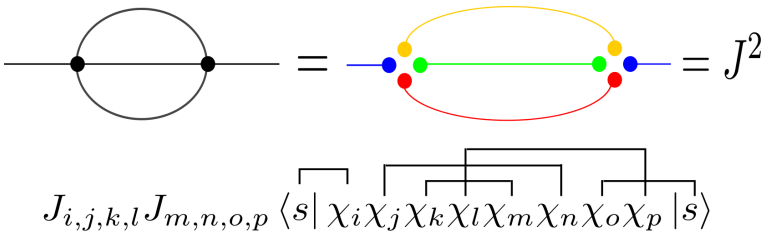

Figure 2.5: *a) This so called melon diagram equals J^2. Note that the two vertices can be brought into the same form by an odd permutation. The minus sign resulting from this cancels the one coming from "untangling" the contractions of the fermionic fields.*

corresponding to $\langle \chi_1 \chi_1 \rangle$ appearing at the second order in the perturbative expansion.

In the figure 2.5 the yellow colour represents the fixed index 1 and the other colours represent the free indices. When the free indices are summed over from 1 to N, we get a factor of N^3 cancelling that from averaging the contributions of the vertices over the Gaussian ensemble. As another example, in the diagram of the figure 2.6, we can only choose the vertices so that there are two free indices (coloured green and red in the figure) or otherwise we end up with odd amount of vertices with the same colours and the contribution of the diagram vanishes when averaged over the probability distribution. Therefore we get a contribution of order $1/N^4$ from the non-melonic diagram of the figure 2.6.

Thus in the limit $N \to \infty$, the contribution of the diagram of figure 2.6 vanishes, but that of figure 2.5 does not. This is an example of a more general fact: only the iterated melonic diagrams contribute to the two-point function in the large N limit.

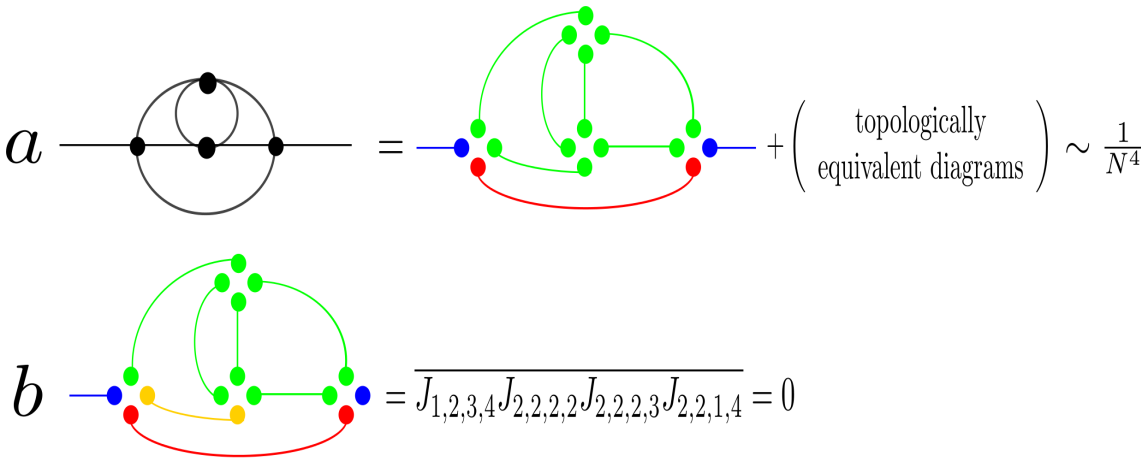

Figure 2.6: *a) A non-melonic diagram giving a contribution of order* $1/N^4$.

b) Even though it might seem at first that we could choose more colours to the diagram a, this is not the case. If we for example try to replace one green line with a yellow line, we find that we get an odd amount of every type of vertex, which leads to a zero contribution when averaged over the Gaussian distribution. It is easy to see that if we try to replace more green lines with yellow ones, we will get a non-zero contribution only once we have replaced every green line with a yellow one. Therefore the maximal number of free indices (colours) is indeed 2.

2.3 Melonic Dominance in the Large N Limit

By an iterated melonic diagram we mean a diagram which can be generated by the following iterative procedure:

1. Begin with a melon diagram (see figure 2.7a).
2. Replace a line between two vertices or vertex and an endpoint with a melonic diagram of the figure 2.7a (see figure 2.7b).
3. Continue replacing lines with melonic diagrams until the diagram is ready.

Any diagram created this way is called an iterated melonic diagram. We also include the free propagator, diagrammatically denoted as a single line among the iterated melonic diagrams. Occasionally iterated melonic diagrams are also referred to as simple melonic diagrams or melon diagrams. It should be clear from the context which kind of a diagram this refers to. Diagrams that cannot be constructed using

this iterative procedure are called non-melonic diagrams.

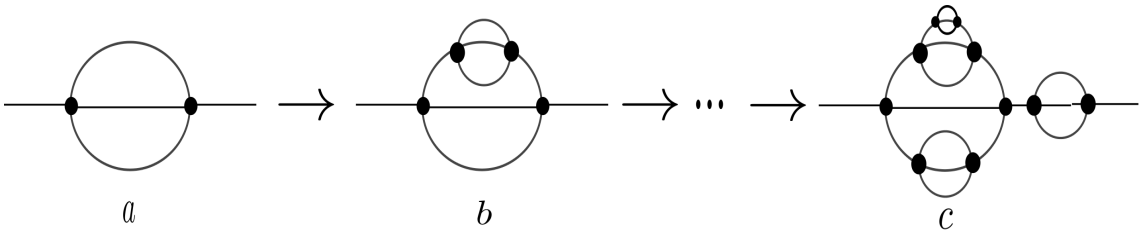

Figure 2.7: *Generating an iterated melonic diagram.*

To prove that the in the $N \to \infty$ limit only the iterated melonic diagrams contribute, we need to prove that the melonic diagrams give a finite contribution i.e. they give a term of order N^0 and the non-melonic diagrams give a term of order N^{-a} for some $a > 0$.

Theorem 2.3.1. *Iterated melonic diagrams give a finite nonzero contribution in the limit $N \to \infty$.*

Proof. We prove this by considering the iterative process by which every iterated melonic diagram can be constructed and show that any diagram generated by this process gives a finite nonzero contribution.

First, based on the previous discussion (see figure 2.5), we know that a melonic diagram of step 1. gives a nonzero contribution. Let us now consider the step where a line is replaced with a melon. As discussed earlier, to get a nonzero contribution, both vertices must be connected to an endpoint with the same colour as the original line (see figure 2.8). This leaves three yet uncoloured endpoints in both vertices. To create an iterated melonic diagram, we must now connect the vertices to each other. Therefore we are free to choose three new colours and connect each endpoint in the first new vertex to the endpoint with the same colour in the other vertex.

The two new vertices give a contribution of order $1/N^3$ when averaging over the disorder. We must also sum over the three new colours, so we get a contribution of N^3 from the sums. These contributions cancel each other, so we get a contribution

of order N^0. Therefore, if the contribution of the original diagram was finite and nonzero, the new diagram will also give a finite nonzero contribution.

Thus we have proven the theorem by induction. □

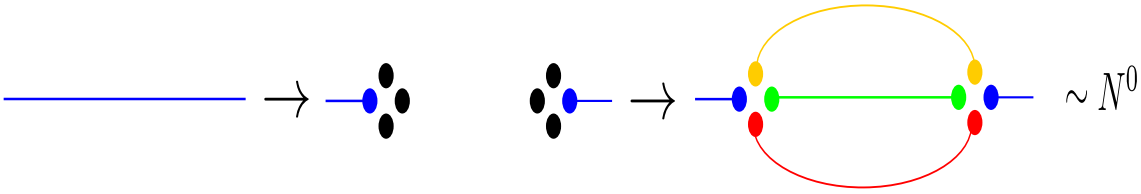

Figure 2.8: *Choosing colours for an iterated melonic diagram.*

Theorem 2.3.2. *Non-melonic diagrams give a zero contribution in the limit $N \to \infty$.*

Proof. We can prove the theorem by considering constructing an arbitrary diagram with n vertices and proving that every diagram that gives a nonzero contribution of order N^0 is necessarily an iterated melonic diagram. To do this, let us consider a collection of n uncoloured vertices. We can, without loss of generality, assume that n is even, since an odd amount of vertices always gives a zero contribution when averaged over the probability distribution. We can then denote $n = 2m$. When averaging over the Gaussian probability distribution, each pair of vertices gives a contribution of order $1/N^3$. Each free index (each new colour) gives a contribution of order N when summed over. There are no other contributions to the powers of N.

Let us first prove that the maximum order of N for any two-point function is N^0. If this was not the case, the diagram with $2m$ vertices would need to have over $3m$ different colours, since the vertices give a contribution of $1/N^{3m}$. On the other hand, we know that the coloured vertices must come in pairs in order to not to give a factor of zero. Therefore with $2m$ vertices we can choose colours for m vertices. In order to have over $3m$ different colours, at least one pair of vertices would then need to have 4 colours that are not present in any other vertex. But then those

two vertices can be only connected to each other, and the resulting diagram would not be fully connected and thus would not contribute to the two-point function [13]. This proves the claim.

Let us then consider a diagram with an arbitrary number of vertices such that it gives a contribution of order N^0. It is clear that such diagram must be of the form displayed in the figure 2.9a. Let us now prove that such diagram must in fact be an iterated melonic diagrams.

To do this, we can prove that any diagram, where there are two vertices connected to each other with two lines, gives a subleading contribution. Any diagram with two vertices which are connected to each other with two lines can be written in the form seen in the figure 2.9b. We can choose 2 new colours for the lines that connect the two vertices in the middle (green and blue in the figure 2.9b).

Clearly, to get a contribution of the maximal order in N, we need to choose the two vertices connected to each other with two lines to be each other's "pairs" (i.e. to have the endpoints with same colours). This is due to the fact that the pair of vertices connected to each other with two lines must have at least two colours in common. If they were not each other's pairs, we would need to have two more vertices that share the two colours that the two vertices connected to each other with two lines have in common. This would clearly lead to less different colours than in the case where the two vertices connected with two lines are each other's pairs and we do not need to have any additional vertices having endpoints with the colours of the lines that the two vertices are connected to each other with.

We can choose 2 more colours (red and yellow in the figure 2.9b) for the lines connecting these vertices to the black box, representing an arbitrary diagram. Then, as a whole the vertices and lines give a contribution of order N. Then the black box contains still $2m$ vertices. The vertices represented by the box must be all connected to each other. In addition, the vertices must again come in pairs having the same colours. As discussed previously, this leaves us with $3m$ yet uncoloured endpoints

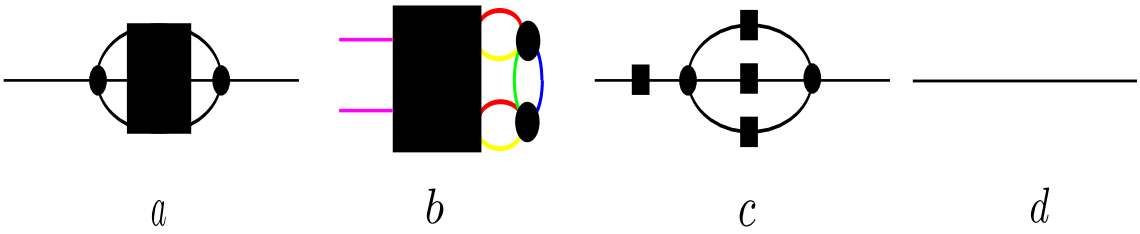

Figure 2.9: *a) Leading-order contributions to the two-point function must be of this form. The black box represents an arbitrary diagram.*

b)Given an arbitrary diagram with two vertices connected to each other, we can choose two colours, green and blue, for the lines connecting the two vertices. Then we can choose two more colours, red and yellow for the lines connecting this pair of vertices to the rest of the diagram.

c and d) The two possible elements that a leading-order diagram can be made of. Any diagram constructed from these elements is clearly an iterated melonic diagram.

that can be coloured with different colours. If we were to colour all these endpoints with different colours, we would get a contribution of order N^0 from the vertices represented by the box. However, connecting the black box to the pair of vertices connected with two lines, we need to use two of these uncoloured endpoints. Then the black box can give at most a contribution of order $1/N^2$. Therefore the total contribution is at most $1/N$, which is subleading.

We have now shown that two vertices can be connected to each other only with three lines or a single line if the resulting diagram is give a contribution of order N^0. Therefore two vertices in leading-order diagrams can be connected to each other only by two ways, with a single line or three lines (figure 2.9c and d). All lines must be connected to another vertex (possibly passing by more vertices) since a vertex that has a line going to itself will clearly result in a subleading diagram. It now easy to see that only diagrams that can be constructed from the elements of the figures 2.9c and 2.9d are melonic. This concludes the proof.

□

2.4 Two-point Function

The free two-point function for the SYK model, $G_0(t_1, t_2)$, is defined by [3, 14]:

$$G_0(t_1, t_2)\delta_{ij} \equiv -\langle T\chi_i(t_1)\chi_j(t_2)\rangle = -\frac{1}{2}\text{sgn}(t_1 - t_2)\delta_{ij}. \tag{2.4.1}$$

The sign is due to the fermionic statistics. Note that $G_0(t, 0)$ is a Green's function of the differential operator $-\partial_t$. This can be seen with a straightforward computation:

$$-\partial_t G_0(t, 0) = \partial_t \left(\frac{1}{2}\text{sgn}(t)\right) = \partial_t \left(\theta(t) - \frac{1}{2}\right) = \delta(t). \tag{2.4.2}$$

In the large N limit also the full two-point function $G(t_1, t_2)$ and the self-energy (the sum of amputated 1-point irreducible diagrams) $\Sigma(t_1, t_2)$ are easy to calculate, since only the iterated melonic diagrams contribute to the expressions for these functions. We now present several different ways of calculating the two-point function in the infrared limit, following [3] and [14].

Due to the existence of an iterative procedure which can be used to generate the contributing diagrams, we can easily express the self-energy in terms of the full two-point function as (see figure 2.10b):

$$\Sigma(t_1, t_2) = J^2 G(t_1, t_2)^3. \tag{2.4.3}$$

We can also derive a recursion relation (Schwinger-Dyson equation) for the two-point function $G(t_1, t_2)$ (figure 2.10c):

$$\begin{aligned} G(t_1, t_2) &= G_0(t_1, t_2) + J^2 \int dt_a dt_b G_0(t_1, t_a) G(t_a, t_b)^3 G(t_b, t_2) \\ &= -\frac{1}{2}\text{sgn}(t_1 - t_2) - J^2 \int dt_a dt_b \frac{1}{2}\text{sgn}(t_1 - t_a) G(t_a, t_b)^3 G(t_b, t). \end{aligned} \tag{2.4.4}$$

This equation can be solved analytically in the infrared limit (i.e. the low energy limit, where $\omega \to 0$) or equivalently in the strong coupling limit, where the time separation t and the constant related to the coupling strength J satisfy $J|t| \to \infty$. It is then self-consistent, as we will show, to assume that the full two-point function $G(t_1, t_2)$ should be negligible compared to the other terms in (2.4.4), so we get an equation

$$\text{sgn}(t_1 - t_2) = -J^2 \int dt_a dt_b \text{sgn}(t_1 - t_a) G(t_a, t_b)^3 G(t_b, t_2). \tag{2.4.5}$$

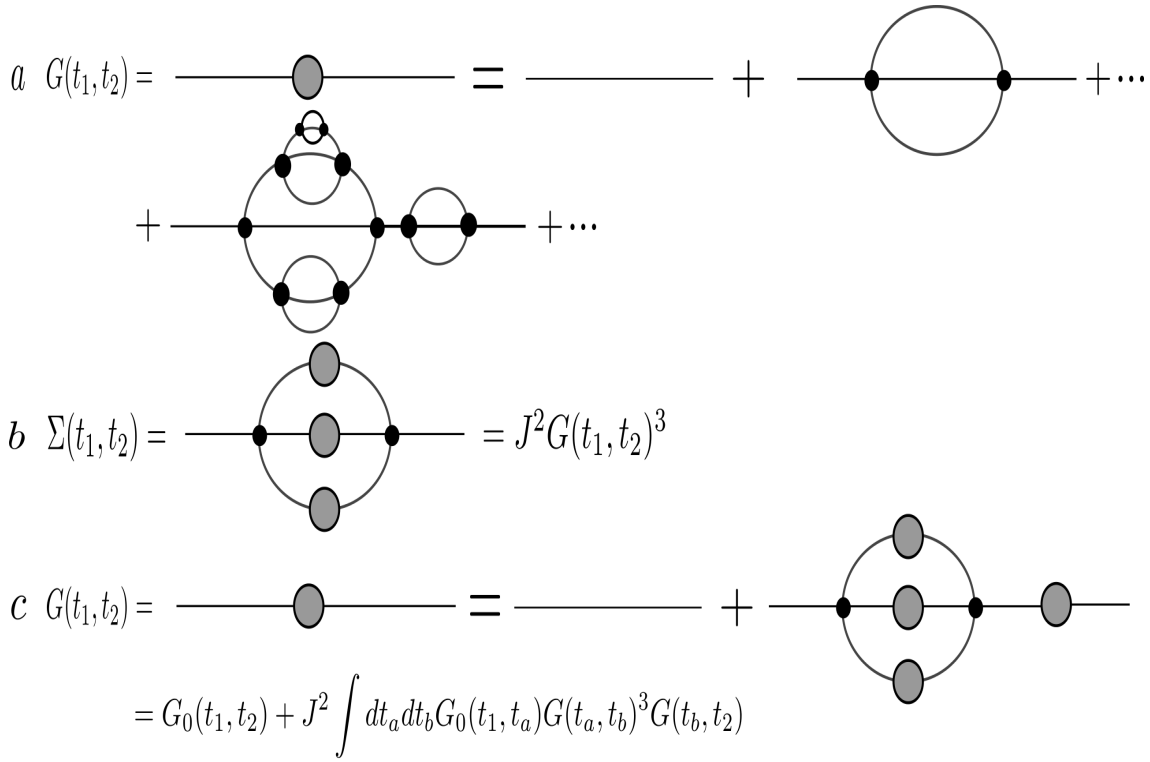

Figure 2.10: *a) The full two-point function $G(t_1, t_2)$, denoted diagrammatically as a grey circle, consists of the sum of all iterated melonic diagrams.*

b) The self-energy corresponds to the sum of all amputated 1-point irreducible diagrams. This means that we only sum over diagrams such that they cannot be split into two distinct diagrams by removing one propagator (line), and that does not have external legs corresponding to the free two-point functions $G_0(t_1, t_2)$. The self-energy can be expressed with the help of the full two-point functions. Here again the grey circles formally denote the sum over all melonic diagrams. The resulting expression for the self-energy is to be read as a sum of all diagrams where the grey circles have been replaced with any iterated melonic diagram (this diagram can be different for every circle).

c) The recursion relation (Schwinger-Dyson equation) for the two-point function. The second diagram on the right-hand side of the equation represents the sum of all diagrams where the grey circles have been replaced by an arbitrary iterated melonic diagram (it can be a different one for every circle). It is rather straightforward to check that this sum gives all the iterated melonic diagrams with the exception of the free two-point function denoted by a simple line. Therefore the sum of all iterated melonic diagrams, which, by definition, is the two-point function $G(t_1, t_2)$, is equal to the two terms on the right-hand side.

This integral equation can be solved for example by trial and error but there is also another, less tedious, way to derive the solution which lends itself much more readily to generalizations, which we shall investigate briefly in the section 3. We can first write the Fourier transformation of the two-point function $G(i\omega)$ in terms of the self-energy. Here the Fourier transformation is done with respect to t_1, keeping t_2 fixed.

$$G(i\omega)^{-1} = -i\omega - \Sigma(i\omega). \tag{2.4.6}$$

Where we used

$$G_0(i\omega) = -\frac{1}{i\omega}. \tag{2.4.7}$$

In the infrared limit ($\omega \to 0$), we can drop $i\omega$ to get

$$-1 = G(i\omega)\Sigma(i\omega) = J^2 G(i\omega)\mathcal{F}[G(t_1,t_2)^3](i\omega), \tag{2.4.8}$$

where $\mathcal{F}\left[G(t_1,t_2)^3\right](i\omega)$ denotes the Fourier transformation of $G(t_1,t_2)^3$ with respect to t_1.

Since $G(t_1,t_2)$ is time translation invariant (and therefore so is $\Sigma(t_1,t_2)$), it can only depend on the difference $t_1 - t_2$ so, we can write $G(t_1,t_2) = G(t_1-t_2)$ and $\Sigma(t_1,t_2) = \Sigma(t_1-t_2)$. By redefining t_1 appropriately, we can take $t_2 = 0$ without loss of generality to simplify the calculations.

Taking the inverse Fourier transformation of (2.4.8) with respect to t, we get

$$-\delta(t) = \int dx \Sigma(x,0)G(t-x,0) = \int dx \Sigma(x-0)G(t-x) = \int dx G(t,x)\Sigma(x,0). \tag{2.4.9}$$

We can also reintroduce t_2 by setting $t = t_1 - t_2$. Doing this and shifting the integration variable $x \to x + t_2$, we get

$$-\delta(t_1 - t_2) = \int dx G(t_1,x)\Sigma(x,t_2). \tag{2.4.10}$$

Substitutig the self-energy $\Sigma(t,t_2)$ in terms of the two-point function from (2.4.3) gives an integral equation:

$$\delta(t_1 - t_2) = -J^2 \int dt G(t_1,t)G(t,t_2)^3. \tag{2.4.11}$$

From this form, we can show that the two-point function $G(t_1, t_2)$ is conformally invariant: If $G(t, t')$ is a solution to (2.4.11), under an arbitrary time reparametrization $t_i = f(s_i)$, we get a new solution if we let

$$G(s, s') = \left|\frac{df(s)}{ds}(s)\right|^{1/4} \left|\frac{df(s)}{ds}(s')\right|^{1/4} G(f(s), f(s')). \tag{2.4.12}$$

This can be seen with a following simple calculation. Let us assume that $G(t_t, t_2)$ satifies (2.4.11). Let us then reparametrize time by setting $t_i = f(s_i)$, where $f(s)$ is a monotonically increasing function. Now (2.4.11) becomes:

$$\delta(f(s_1) - f(s_2)) = -J^2 \int dt G(f(s_1), t) G(t, f(s_2))^3. \tag{2.4.13}$$

Now we can use the delta-function identity:

$$\delta(f(s_1) - f(s_2)) = \frac{\delta(s_1 - s_2)}{|\frac{df}{ds}(s_1)|}. \tag{2.4.14}$$

Since the delta-function sets $s_1 = s_2$, we can express this as:

$$\delta(f(s_1) - f(s_2)) = \frac{\delta(s_1 - s_2)}{|\frac{df}{ds}(s_1)|^{1/4} |\frac{df}{ds}(s_2)|^{3/4}}. \tag{2.4.15}$$

Using this and $dt = \frac{dt}{ds}(s)ds = \frac{df}{ds}(s)ds = |\frac{df}{ds}(s)|ds$, where the last equality follows because $f(s)$ is monotonically increasing, we get that

$$\frac{\delta(s_1 - s_2)}{\left|\frac{df}{ds}(s_1)\right|^{1/4} \left|\frac{df}{ds}(s_2)\right|^{3/4}} = -J^2 \int ds \left|\frac{df}{ds}(s)\right| G(f(s_1), f(s)) G(f(s), f(s_2))^3. \tag{2.4.16}$$

Rearranging, we find that

$$\begin{aligned}\delta(s_1 - s_2) = -J^2 \int ds &\left|\frac{df}{ds}(s_1)\right|^{1/4} \left|\frac{df}{ds}(s)\right|^{1/4} G(f(s_1), f(s)) \\ &\times \left(\left|\frac{df}{ds}(s)\right|^{1/4} \left|\frac{df}{ds}(s_2)\right|^{1/4} G(f(s), f(s_2))\right)^3.\end{aligned} \tag{2.4.17}$$

Now using the definition (2.4.12), we find that we can express this simply as

$$\delta(s_1 - s_2) = -J^2 \int ds G(s_1, s) G(s, s_2)^3. \tag{2.4.18}$$

This is exactly the same as (2.4.11), which, with definition (2.4.12), proves the invariance under the reparametrizations.

We will need the fact that the two-point function is conformally invariant later when investigating the four-point function. Now the two-point function can be calculated by using either equation (2.4.8) or (2.4.11). Let us do this by using the former. The form of the equation (2.4.8) suggests a power-law two-point function as a good trial function. It turns out, however, that a correct solution is not, in fact, a power law but "almost a power law". Let us try a function of the form:

$$G(t_1, t_2) = C|t_1 - t_2|^x \text{sgn}(t_1 - t_2). \tag{2.4.19}$$

Without loss of generality, we can set $t_1 = t$ and $t_2 = 0$ to get

$$G(t, 0) = C|t|^x \text{sgn}(t). \tag{2.4.20}$$

Calculating the Fourier transform of the trial function $G(t, 0)$, we find that

$$G(i\omega) = \int dt e^{i\omega t} C|t|^x \text{sgn}(t) = 2iC \ \text{sgn}(\omega) \cos\left(\frac{\pi x}{2}\right) \Gamma(1-x) \, |\omega|^{x-1} . \tag{2.4.21}$$

Similarly for the self-energy:

$$\Sigma(i\omega) = J^2 \int dt e^{i\omega t} C^3 |t|^{3x} \text{sgn}(t) = 2iJ^2C^3 \ \text{sgn}(\omega) \cos\left(\frac{3\pi x}{2}\right) \Gamma(1-3x) \, |\omega|^{3x-1} . \tag{2.4.22}$$

Substituting these to the equation (2.4.8), we get that

$$-1 = -4J^2C^4 \cos\left(\frac{3\pi x}{2}\right) \cos\left(\frac{\pi x}{2}\right) \Gamma(1-x)\Gamma(1-3x) \, |\omega|^{4x-2} , \tag{2.4.23}$$

where we have noted that the sign-functions cancel each other. To get a correct functional dependence on ω, we must have $x = 1/2$. Then the equation above reads:

$$-1 = -4J^2C^4\pi. \tag{2.4.24}$$

Solving for C now gives

$$C = -\left(\frac{1}{4\pi J^2}\right)^{1/4} , \tag{2.4.25}$$

where we have chosen the negative root. Therefore the two-point function $G(t_1, t_2)$ is given by:

$$G(t_1, t_2) = -\left(\frac{1}{4\pi J^2}\right)^{1/4} \frac{1}{\sqrt{|t_1 - t_2|}} \text{sgn}(t_1 - t_2). \tag{2.4.26}$$

The late time decay of the full two-point function (2.4.26) shows that the approximation where $G(0,t)$ was dropped from the left-hand side of the Schwinger-Dyson equation (2.4.4), or equivalently dropping $i\omega$ from (2.4.6), was self-consistent.

It is easy to check that this solution also satisfies (2.4.11) and (2.4.5). To do the latter, we would need to calculate the integral:

$$-J^2 \int dt_a dt_b \mathrm{sgn}(t_1-t_a) G(t_a,t_b)^3 G(t_b,t_2) = \frac{1}{4\pi} \int dt_1 dt_2 \mathrm{sgn}(t_1-t_a) \frac{\mathrm{sgn}(t_a-t_b)}{|t_a-t_b|^{3/2}} \times \frac{\mathrm{sgn}(t_b-t_2)}{|t_b-t_2|^{1/2}}. \tag{2.4.27}$$

This integral is actually divergent but it can be analytically continued and then shown to satisfy the equation (2.4.27), using methods similar to those from section 2.5.2.

2.5 Four-point Function

The most general four-point function of SYK model is defined as:

$$\langle \chi_i(t_1)\chi_i(t_2)\chi_j(t_3)\chi_j(t_4)\rangle \tag{2.5.1}$$

We will, however, consider a slightly more convenient correlator, following [14], where the different choices of indices i and j are averaged over, given by

$$\frac{1}{N^2}\sum_{i,j=1}^{N} \langle T\left(\chi_i(t_1)\chi_i(t_2)\chi_j(t_3)\chi_j(t_4)\right)\rangle = G(t_1,t_2)G(t_3,t_4) + \frac{1}{N}\Gamma(t_1,t_2,t_3,t_4) + O(\frac{1}{N^2}). \tag{2.5.2}$$

Here we have chosen the prefactor of $\Gamma(t_1,t_2,t_3,t_4)$ so that we will have $\Gamma(t_1,t_2,t_3,t_4) = O(N^0)$. This means that $\Gamma(t_1,t_2,t_3,t_4)$ consists of all contributions of order $O(N)$ divided by N. We will consider the leading-order correction $\Gamma(t_1,t_2,t_3,t_4)$ to the four-point function. The leading-order diagrams in the large N limit contributing to $\Gamma(t_1,t_2,t_3,t_4)$ consist of so-called ladder diagrams (figure 2.11) that can be created

with the following iterative process:

1. Begin with a diagram of the figure 2.11a or 2.11b.
2. Add a vertex to both lines.
3. Connect new vertices to each other with two lines.
4. Add two-point propagators to all lines that do not yet have them. This results in a diagram in the figure 2.11c or 2.11d.
5. Repeat from step 2 until ready.

As a special case we also include so called "zero-rung ladders", i.e. the diagrams of the figure 2.11a and 2.11b, among ladder diagrams. It can be proven that all the ladder diagrams give a contribution of order $1/N$ and all other diagrams give a contribution of order $1/N^2$ or lower. The proof is similar to the one presented for the iterated melonic diagrams in the case of the two-point function. As an example, let us consider two diagrams contributing to the four-point function - one ladder diagram and the other not (see figure 2.12). In the case of the zero-rung ladders the contribution of order $O(N^{-1})$ is due to the propagators setting $i = j$ and thus giving one free index less than a product of two propagators would usually give.

2.5.1 Recursion Relation for the Ladder Diagrams

It is again easy to derive a recursion relation (Schwinger-Dyson equation) for these diagrams. Let us denote the sum of all ladder diagrams (including the ladder diagram with no rungs, which is just a product of two two-point functions) by $\Gamma(t_1, t_2, t_3, t_4)$. This is just the sum over the ladder diagrams with a different number of rungs:

$$\Gamma(t_1, t_2, t_3, t_4) = \sum_{n=1}^{\infty} \Gamma_n(t_1, t_2, t_3, t_4). \tag{2.5.3}$$

Clearly a ladder diagrams with $n+1$ rungs can be expressed as a ladder diagram with one rung times a ladder diagram with n rungs if integrate over all times connecting

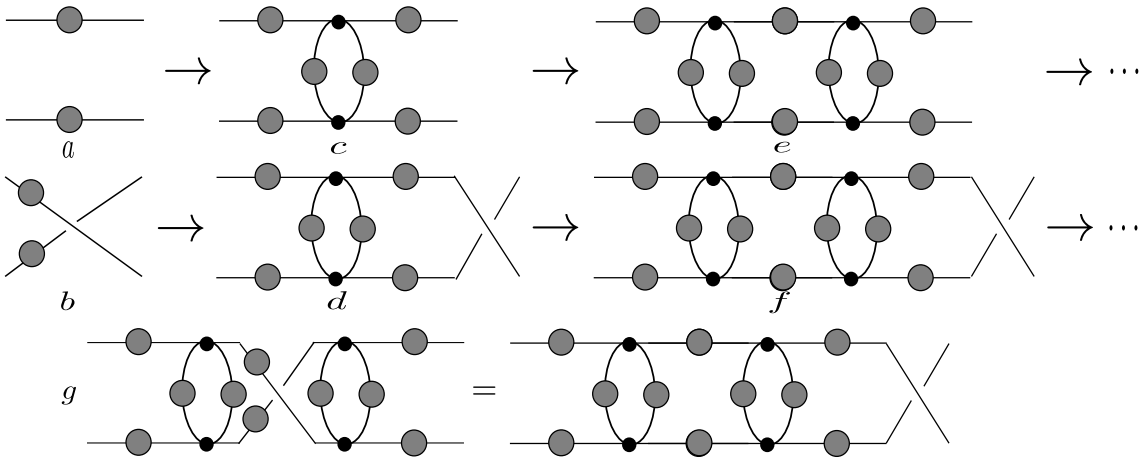

Figure 2.11: *a-f) Generating ladder diagrams iteratively. The grey circle represents again the two-point function. The vertical double lines from one vertex to another are called rungs and the horizontal lines from one endpoint to another are called rails. A sum of the two possible ladder diagrams with n rungs is denoted also by* $N\Gamma_n(t_1, t_2, t_3, t_4)$ *(the N is due to our convention of defining* $\Gamma_n(t_1, t_2, t_3, t_4)$ *so that it is of the order* $O(N^0)$*). For example, the sum of the ladder diagram (c) and (d), which both have one rung, is equal to* $N\Gamma_1(t_1, t_2, t_3, t_4)$ *and the sum of the diagrams (e) and (f), which have two rungs, equal* $N\Gamma_2(t_1, t_2, t_3, t_4)$*. Diagrams (c) and (d) have two rails and (e) and (f) three.*

g) We only need to include the ladder diagrams that have crossing propagators between the last rung and the endpoints, such as diagrams (d) and (f), or no crossing propagators at all, such as (b) and (e). This is due to the fact that all other types of diagrams are equivalent to either of these types. To see this, we need just to note that by "twisting" nth rung, we can bring crossing propagators between $n-1$*th and nth rung to between nth and* $n+1$*th rung. This allows us to bring the crosses to after the last rung. Let us also note that if we bring two crosses to after the last rung, they will cancel each other. Therefore it follows that the diagrams with an odd number of crosses are all equivalent to a diagram with crossing propagators between the last rung and endpoints. The diagrams with an even number of crosses are equivalent to diagrams with no crossing propagators at all.*

the two diagrams. The two ladder diagrams also contribute two pairs of propagators between two ladder diagrams, so we have to omit the other pair (see figure 2.13b). We have also to note that there are two ladder diagrams with n rungs (see figure 2.13b) so we have to multiply the both diagrams with a new part with one new rung if we want to generate all the ladder diagrams with $n + 1$ rungs. Therefore we find

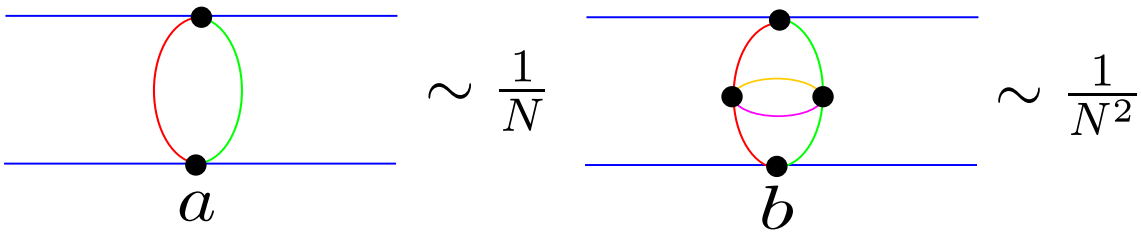

Figure 2.12: *a) A ladder diagram gives a contribution of order* $1/N$.
b) A non-ladder diagram giving a contribution of $1/N^2$.

that

$$\Gamma_{n+1}(t_1,t_2,t_3,t_4) = -\int dt_a dt_b 3J^2 G(t_1,t_a)G(t_2,t_b)G(t_a,t_b)^2\Gamma_n(t_a,t_b,t_3,t_4). \quad (2.5.4)$$

This equation can be written as:

$$\Gamma_{n+1}(t_1,t_2,t_3,t_4) = \int dt_a dt_b K(t_1,t_2,t_a,t_b)\Gamma_n(t_a,t_b,t_3,t_4), \quad (2.5.5)$$

where we introduced the kernel $K(t_1,t_2,t_3,t_4)$ defined by:

$$K(t_1,t_2,t_3,t_4) = -3J^2 G(t_1,t_3)G(t_2,t_4)G(t_3,t_4)^2. \quad (2.5.6)$$

Therefore we can generate all the ladder diagrams by multiplying the sum of the two types of ladder diagrams with no rungs, $\Gamma_0(t_1,t_2,t_3,t_4)$, by the kernel $K(t_1,t_2,t_3,t_4)$. The sum of ladder diagrams $\Gamma_0(t_1,t_2,t_3,t_4)$ is just an antisymmetrized product of propagators:

$$\Gamma_0(t_1,t_2,t_3,t_4) = G(t_1,t_4)G(t_2,t_3) - G(t_1,t_3)G(t_2,t_4). \quad (2.5.7)$$

To find out the leading-order correction to the four-point function, we need to find an explicit expression for the sum of the ladder diagrams, $\Gamma(t_1,t_2,t_3,t_4)$. This is easier if we first diagonalize the kernel (2.5.6). In order to do this, we can first compute its eigenvalues and eigenfunctions. We do this by showing that the eigenfunctions of the $SL(2)$ Casimir operator acting on t_1 and t_2 are also the eigenfunctions of the kernel. Then we proceed to find the eigenfunctions of the Casimir operator. It turns out that the eigenfunctions can be expressed as a superposition of rather simple solutions. For this reason it is useful to analyze first a simple set of eigenvectors which turn out to have the form of the components of the superposition.

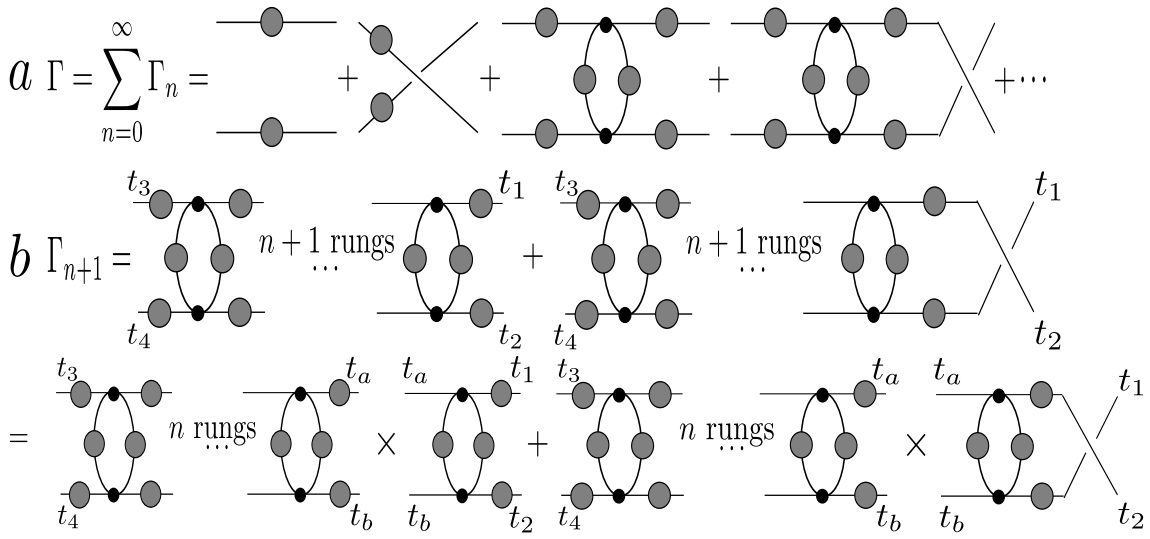

Figure 2.13: *a) The sum of all the ladder diagrams, $\Gamma(t_1, t_2, t_3, t_4)$, includes all the ladder diagrams with an arbitrary amount of rungs and their antisymmetrized versions.*

b) The recursion relation for the ladder diagrams. We can generate a ladder with $n+1$ rungs by multiplying both n-rung ladders with the kernel.

2.5.2 A Particular Set of Eigenfunctions

The eigenfunctions $v_\alpha(t_a, t_b)$ of $K(t_3, t_4, t_a, t_b)$ must satisfy:

$$\begin{aligned} g(\alpha)v_\alpha(t_1, t_2) &= \int dt_a dt_b K(t_1, t_2, t_a, t_b) v_\alpha(t_a, t_b) \\ &= \frac{3}{4\pi} \int dt_a dt_b \frac{\mathrm{sgn}(t_1 - t_a)}{|t_1 - t_a|^{1/2}} \frac{\mathrm{sgn}(t_2 - t_b)}{|t_2 - t_b|^{1/2}} \frac{1}{|t_a - t_b|} v_\alpha(t_a, t_b). \end{aligned} \tag{2.5.8}$$

for some $g(\alpha)$, which can depend on t_1 and t_2.

We see that this integral has some similarities with an earlier integral equation (2.4.27) for which the solution was given by (2.4.26). We can try a similar trial function in this case. We will next show that a particular set of solutions is given by

$$v_\alpha(t_a, t_b) = \frac{1}{|t_a - t_b|^{1/2 - 2\alpha}} \mathrm{sgn}(t_a - t_b), \tag{2.5.9}$$

where the exponent has been chosen to have this form in order to make the connection to the general eigenfunctions, which we will find later, more explicit. To prove

that (2.5.9) are really eigenvectors of the kernel, (2.5.6), we need to show that:

$$g(\alpha)\frac{1}{|t_1-t_2|^{1/2-2\alpha}}\mathrm{sgn}(t_1-t_2) = -\frac{3}{4\pi}\int dt_a dt_b \frac{\mathrm{sgn}(t_1-t_a)}{|t_1-t_a|^{1/2}}\frac{\mathrm{sgn}(t_2-t_b)}{|t_2-t_b|^{1/2}}\frac{\mathrm{sgn}(t_a-t_b)}{|t_a-t_b|^{3/2-2\alpha}}. \tag{2.5.10}$$

This integral is, like (2.4.27), divergent, but we can analytically continue it. To do this, it is useful to remember the following identities for the beta-function:

$$\int_{-\infty}^{b} dt \frac{1}{(a-t)^x}\frac{1}{(b-t)^y} = \frac{1}{(a-b)^{x+y-1}}\beta(1-y, x+y-1), \tag{2.5.11}$$

$$\int_{a}^{\infty} dt \frac{1}{(t-a)^x}\frac{1}{(t-b)^y} = \frac{1}{(a-b)^{x+y-1}}\beta(1-x, x+y-1), \tag{2.5.12}$$

$$\int_{a}^{b} dt \frac{1}{(t-a)^x}\frac{1}{(b-t)^y} = \frac{1}{(b-a)^{x+y-1}}\beta(1-x, 1-y). \tag{2.5.13}$$

Let us now consider a general integral of the form

$$\int dt_a dt_b \frac{\mathrm{sgn}(t_1-t_a)}{|t_1-t_a|^x}\frac{\mathrm{sgn}(t_2-t_b)}{|t_2-t_b|^x}\frac{\mathrm{sgn}(t_a-t_b)}{|t_a-t_b|^y}, \tag{2.5.14}$$

so that we recover the special case (2.5.10) by substituting $x = 1/2$ and $y = 3/2-2\alpha$.

We can now split the integration interval into separate parts - one for every combination of the values of sgn-functions. For example, in the case $t_1 > t_2$ we split the integrals as follows:

$$\begin{aligned}&\int_{-\infty}^{\infty} dt_a \int_{-\infty}^{\infty} dt_b \to \int_{-\infty}^{t_2} dt_b \left(\int_{-\infty}^{t_b} dt_a + \int_{t_b}^{t_1} dt_a + \int_{t_1}^{\infty} dt_a\right)\\ &+\int_{t_2}^{t_1} dt_b \left(\int_{-\infty}^{t_b} dt_a + \int_{t_b}^{t_1} dt_a + \int_{t_1}^{\infty} dt_a\right)+\int_{t_1}^{\infty} dt_b \left(\int_{-\infty}^{t_1} dt_a + \int_{t_1}^{t_b} dt_a + \int_{t_b}^{\infty} dt_a\right).\end{aligned} \tag{2.5.15}$$

Let us calculate one term explicitly in case $t_1 > t_2$:

$$\begin{aligned}&\int_{t_1}^{\infty} dt_a \int_{t_2}^{t_1} dt_b \frac{\mathrm{sgn}(t_1-t_a)}{|t_1-t_2|^x}\frac{\mathrm{sgn}(t_2-t_b)}{|t_2-t_b|^x}\frac{\mathrm{sgn}(t_a-t_b)}{|t_a-t_b|^y}\\ &= \int_{t_1}^{\infty} dt_a \int_{t_2}^{t_1} dt_b \frac{1}{(t_a-t_1)^x}\frac{1}{(t_b-t_2)^x}\frac{1}{(t_a-t_b)^y}\\ &= \int_{t_1}^{\infty} dt_a \frac{1}{(t_a-t_1)^x}\frac{1}{(t_a-t_2)^{x+y-1}}\beta(1-x,1-y)\\ &= \frac{1}{(t_1-t_2)^{2x+y-2}}\beta(1-x,2x+y-2)\beta(1-x,1-y).\end{aligned} \tag{2.5.16}$$

Calculating contributions from all the intervals in a similar fashion and summing them all up gives a result, in case $t_1 > t_2$:

$$
\begin{aligned}
&-\frac{3}{4\pi}\int dt_a dt_b \frac{\operatorname{sgn}(t_1-t_a)}{|t_1-t_a|^x}\frac{\operatorname{sgn}(t_2-t_b)}{|t_2-t_b|^x}\frac{\operatorname{sgn}(t_a-t_b)}{|t_a-t_b|^y} = -\frac{3}{4\pi}\frac{1}{|t_3-t_4|^{2x+y-2}} \\
&\times\Big(\beta(1-x,1-y)\beta(1-x,2x+y-2)-\beta(1-x,x+y-1)\beta(1-x,2x+y-2) \\
&-\beta(1-x,1-y)\beta(1-x,2-x-y)+\beta(1-x,1-y)\beta(1-x,2x+y-2) \\
&-\beta(1-x,1-y)\beta(2-x-y,2x+y-2)+\beta(1-x,x+y-1)\beta(2-x-y,2x+y-2) \\
&+\beta(1-y,x+y-1)\beta(1-x,2-x-y)-\beta(1-x,1-y)\beta(2-x-y,2x+y-2)\Big).
\end{aligned}
\tag{2.5.17}
$$

Substituting $x = 1/2$ and $y = 3/2 - 2\alpha$ gives then:

$$
\begin{aligned}
&-\frac{3}{4\pi}\int dt_a dt_b \frac{\operatorname{sgn}(t_1-t_a)}{|t_1-t_a|^{1/2}}\frac{\operatorname{sgn}(t_2-t_b)}{|t_2-t_b|^{1/2}}\frac{\operatorname{sgn}(t_a-t_b)}{|t_a-t_b|^{3/2-2\alpha}} \\
&= -\frac{3}{4\pi}\frac{1}{|t_3-t_4|^{1/2-2\alpha}}\frac{4\pi}{4\alpha-1}\cot\left(\pi\left(\frac{3}{4}-\alpha\right)\right).
\end{aligned}
\tag{2.5.18}
$$

We can now substitute this equation into (2.5.10) and simplify:

$$
g(\alpha)\frac{1}{|t_3-t_4|^{1/2-2\alpha}} = \frac{1}{|t_3-t_4|^{1/2-2\alpha}}\frac{3}{4\alpha-1}\tan\left(\pi\left(\alpha-\frac{1}{4}\right)\right). \tag{2.5.19}
$$

Therefore the eigenvalues corresponding to $v_\alpha(t_3,t_4)$ are:

$$
g(\alpha) = \frac{3}{4\alpha-1}\tan\left(\pi\left(\alpha-\frac{1}{4}\right)\right). \tag{2.5.20}
$$

Similar calculation in the case $t_4 > t_3$ gives the same result, so the eigenvalues for eigenfunctions $v_\alpha(t_a,t_b)$ are indeed given by (2.5.20).

2.5.3 A Complete Set of Eigenfunctions

To find a complete set of eigenvectors of the kernel $K(t_1,t_2,t_3,t_4)$, we can use its $SL(2)$ invariance. To see the nature of this invariance, let us define the following generators of the $SL(2)$ algebra:

$$
D_i = -t_i\partial_{t_i} - \frac{1}{4}, \qquad P_i = \partial_{t_i}, \qquad K = t_i^2\partial_{t_i} + \frac{1}{2}. \tag{2.5.21}
$$

It easy to see that they satisfy the following commutation relations:

$$[D_i, P_j] = P_i\delta_{ij}, \qquad [D_i, K_j] = -K_i\delta_{ij}, \qquad [P_i, K_j] = -2D_i\delta_{ij}. \tag{2.5.22}$$

It can be checked [14] that these generators commute with the kernel $K(t_1, t_2, t_3, t_4)$ in the sense that, up to total derivatives, we have the following three relations:

$$(D_1 + D_2)K(t_1, t_2, t_3, t_4) = K(t_1, t_2, t_3, t_4)(D_3 + D_4). \tag{2.5.23}$$

$$(P_1 + P_2)K(t_1, t_2, t_3, t_4) = K(t_1, t_2, t_3, t_4)(P_3 + P_4). \tag{2.5.24}$$

$$(K_1 + K_2)K(t_1, t_2, t_3, t_4) = K(t_1, t_2, t_3, t_4)(K_3 + K_4). \tag{2.5.25}$$

This symmetry implies three things: First, since the kernel $K(t_1, t_2, t_3, t_4)$ is $SL(2)$ invariant, we can represent it as a function of $SL(2)$ invariant cross ratio χ, which is defined by:

$$\chi = \frac{(t_1 - t_2)(t_3 - t_4)}{(t_1 - t_3)(t_2 - t_4)}. \tag{2.5.26}$$

Secondly, it is easy to see from the expression (2.5.7) for $\Gamma_0(t_1, t_2, t_3, t_4)$ that $\Gamma_0(t_1, t_2, t_3, t_4)$ transforms like a conformal four-point function. Since the ladder diagrams with n rungs, $\Gamma_n(t_1, t_2, t_3, t_4)$, are generated by acting on $\Gamma_0(t_1, t_2, t_3, t_4)$ by a $SL(2)$ invariant kernel, the $\Gamma_n(t_1, t_2, t_3, t_4)$ must also transform like a conformal four-point function. In other words, we can write

$$\Gamma_n(t_1, t_2, t_3, t_4) = G(t_1, t_2)G(t_3, t_4)\Gamma_n(\chi), \tag{2.5.27}$$

where $\Gamma_n(\chi)$ is as yet undetermined function that only depends on the cross ratio χ. We will later solve this function (see (2.5.68) for an explicit calculation of $\Gamma_0(\chi)$).

Finally, from the "commutation relations" (2.5.23)-(2.5.25) immediately follows a similar "commutation relation" for the Casimir operator $\mathcal{C}_{1+2}$:

$$\mathcal{C}_{1+2}K(t_1, t_2, t_3, t_4) = K(t_1, t_2, t_3, t_4)\mathcal{C}_{3+4}, \tag{2.5.28}$$

where the Casimir operator $\mathcal{C}_{i+j}$ is defined by

$$\begin{aligned}\mathcal{C}_{i+j} &= (D_i + D_j)^2 - \frac{1}{2}(P_i + P_j)(K_i + K_j) - \frac{1}{2}(K_i + K_j)(P_i + P_j) \\ &= -\frac{8}{3} + 2D_iD_j - P_iK_j - K_iP_j. \end{aligned} \tag{2.5.29}$$

The relation (2.5.28) in turn implies the eigenfunctions of the Casimir operator $\mathcal{C}_{i+j}$ must be also the eigenfunctions of the kernel. This follows straightforwardly from the following observation: Assuming that $v_\alpha(t_1, t_2)$ is an eigenvector of the Casimir operator $\mathcal{C}_{1+2}$ with eigenvalue $c(\alpha)$, we get:

$$\begin{aligned}c(\alpha) \int dt_a dt_b K(t_1, t_2, t_a, t_b) v_\alpha(t_a, t_b) &= \int dt_a dt_b K(t_1, t_2, t_a, t_b) \mathcal{C}_{a+b} v_\alpha(t_a, t_b) \\ &= \mathcal{C}_{1+2} \int dt_a dt_b K(t_1, t_2, t_a, t_b) v_\alpha(t_a, t_b). \end{aligned} \tag{2.5.30}$$

From this, it follows that if the spectrum of the kernel $K(t_1, t_2, t_3, t_4)$ is nondegenarate, so that $\int dt_a dt_b K(t_1, t_2, t_a, t_b) v_\alpha(t_a, t_b) \sim v_\alpha(t_1, t_2)$, then $v_\alpha(t_1, t_2)$ is an eigenfunction of $\mathcal{C}_{1+2}$. We shall show the nondegeracy of the spectrum explicitly later.

2.5.4 Eigenfunctions of the Casimir Operator

As discussed previously, we can write the ladder diagrams in the terms of a function $\Gamma_n(\chi)$ that only depends on the cross ratio by defining

$$\Gamma_n(t_1, t_2, t_3, t_4) = G(t_1, t_2) G(t_3, t_4) \Gamma_n(\chi) \sim \frac{1}{\sqrt{t_1 - t_2}} \Gamma_n \left(\frac{(t_1 - t_2)(t_3 - t_4)}{(t_1 - t_3)(t_2 - t_4)} \right), \tag{2.5.31}$$

where $\sim$ denotes the proportionality to the terms that depend on t_1 or t_2. A straightforward computation shows that the Casimir operator $\mathcal{C}_{1+2}$ acts on this as

$$\mathcal{C}_{1+2} \frac{1}{\sqrt{|t_1 - t_2|}} \Gamma_n \left(\frac{(t_1 - t_2)(t_3 - t_4)}{(t_1 - t_3)(t_2 - t_4)} \right) = \frac{1}{\sqrt{|t_1 - t_2|}} \mathcal{C}_\chi \Gamma_n(\chi), \tag{2.5.32}$$

where the operator $\mathcal{C}_\chi$ is defined by

$$\mathcal{C}_\chi = (\chi^2 - \chi^3)\partial_\chi^2 - \chi^2 \partial_\chi. \tag{2.5.33}$$

To make the evaluation of the sum of all the ladder diagrams easy, we want to find a basis of functions that diagonalises the kernel i.e.are its eigenfunctions and expand $\Gamma_n(\chi)$ in that basis. Since we have shown that the eigenfunctions of the Casimir operator $\mathcal{C}_{1+2}$ are also eigenfunctions of the kernel, we can try to find a suitable basis of the eigenfunctions of the Casimir operator. We denote the eigenvalues of $\mathcal{C}_\chi$ by $2\alpha(2\alpha-1)$ and the eigenfunction corresponding to this eigenvalue by $F_\alpha(\chi)$. To solve the eigenfunctions of $\mathcal{C}_{1+2}$ we can then solve the following eigenvalue equation:

$$2\alpha(2\alpha-1)F(\chi) = \mathcal{C}_\chi F_\alpha(\chi). \tag{2.5.34}$$

In addition we require that $F'_\alpha(2) = 0$ and that the function $F_\alpha(\chi)$ must be normalizable with respect to the following inner product $\langle f, g\rangle$:

$$\langle f, g\rangle = \int_0^2 \frac{d\chi}{\chi} f(\chi)^* g(\chi), \tag{2.5.35}$$

It can be shown [14] that the functions $F_\alpha(\chi)$ with these properties form a complete orthogonal basis (we will show orthogonality later), so we can expand $\Gamma_0(\chi)$ in terms of them.

To see how the condition $F'_\alpha(2) = 0$ (and the integration limits in the inner product above) come about, let us consider the function $\Gamma_n(\chi)$. Directly from the definition of $\Gamma_n(\chi)$ (2.5.27) we see that

$$\Gamma_n(\chi) = \langle T\left(\chi_i(t_1)\chi_i(t_2)\chi_j(t_3)\chi_j(t_4)\right)\rangle. \tag{2.5.36}$$

Note that the cross ratio χ is invariant under the Möbius transformations of the form

$$t \to \frac{at+b}{ct+d} \tag{2.5.37}$$

with $ad - bc \neq 0$. We can use these transformations to set $t_1 = 0$, $t_2 > 0$ $t_3 = 1$, $t_4 \to \infty$ so that $\chi = t_2 > 0$. Then we have that

$$\Gamma_n(\chi) \sim \begin{cases} \langle \chi_j(\infty)\chi_j(1)\chi_i(\chi)\chi_i(0)\rangle & 0 < \chi < 1 \\ -\langle \chi_j(\infty)\chi_i(\chi)\chi_j(1)\chi_i(0)\rangle & 1 < \chi < \infty \end{cases}. \tag{2.5.38}$$

From this form, we can show that we have a symmetry $\chi \to \chi/(\chi-1)$ when $\chi > 1$. To see this, let us consider the following mapping

$$\frac{t-2}{t} = \tan\left(\frac{\theta}{2}\right). \tag{2.5.39}$$

This mapping takes $0 \to -\pi$, $1 \to -\pi/2$, $\infty \to \pi/2$ and $\chi = t_2 = \theta$ for some $-\pi \leq \theta \leq \pi$. Then we have that

$$\Gamma_n(\chi) \sim \langle T\chi_j(\pi/2)\chi_i(\theta)\chi_j(-\pi/2)\chi_i(-\pi)\rangle. \tag{2.5.40}$$

From this form, it is immediately clear that $\theta \to -\theta$ is a symmetry of $\Gamma_n(\chi)$. The mapping $\theta \to -\theta$ corresponds the mapping

$$\frac{t_2-2}{t_2} \to \frac{2-t_2}{t_2}. \tag{2.5.41}$$

Or equivalently

$$\chi \to \frac{\chi}{\chi-1}. \tag{2.5.42}$$

Since the transformation $\chi \to \chi/(\chi-1)$ maps the interval $1 < \chi < 2$ to $2 < \chi$, the full function $\Gamma_n(\chi)$ can be determined from $\Gamma_n(\chi)$ on the interval $0 < \chi < 2$. In addition, we must have $\Gamma_n'(\chi = 2) = 0$ since $\chi = 2$ is the fixed point of the transformation. Since we have $\Gamma_n'(\chi = 2) = 0$, it is natural to require this also of the basis functions $F_\alpha(\chi)$.

The eigenvalue equation (2.5.34) can be transformed into a hypergeometric differential equation whose solution can be given in terms of the hypergeometric functions. The general solution to the eigenequation (2.5.34) is given by

$$F_\alpha(\chi) = A\chi^{2\alpha}{}_2F_1(2\alpha, 2\alpha, 4\alpha, \chi) + B\chi^{1-2\alpha}{}_2F_1(1-2\alpha, 1-2\alpha, 2-4\alpha, \chi), \tag{2.5.43}$$

where the functions ${}_2F_1(a,b,c,z)$ are ordinary hypergeometric functions. The constants A, B and α can be determined from three conditions we set for the eigenfunctions $F_\alpha(\chi)$ above. The overall constant is determined by the normalization of the eigenfunctions.

Let us now find the constants A, B and α so that the general solution to the eigenequation given by $F_\alpha(\chi)$ in (2.5.43) satisfies the three conditions described above. Let us start with the condition $F'(2) = 0$. Taking the first derivative of (2.5.43), we find that

$$F'_\alpha(2) = A\alpha 2^{2\alpha}{}_2F_1(2\alpha, 2\alpha+1, 2\alpha, 2) - B(2\alpha-1)2^{-2\alpha}{}_2F_1(1-2\alpha, 2-2\alpha, 2-4\alpha, 2). \tag{2.5.44}$$

Solving for A (or B) and substituting to (2.5.43), we find that for $1 < \chi < 2$, we have, up to normalization, which we have chosen here so that the expansion of (2.5.45) near $\chi = 1$ has a convenient form, that

$$F_\alpha(\chi) = \frac{\Gamma\left(\frac{1}{2}-\alpha\right)\Gamma(\alpha)}{\sqrt{\pi}}{}_1F_2\left(\alpha, \frac{1}{2}-\alpha, \frac{1}{2}, \frac{(2-\chi)^2}{\chi^2}\right). \tag{2.5.45}$$

We notice that this solution has an obvious symmetry $\chi \to \chi/(\chi-1)$, so we conclude that it is indeed a correct solution for all values $1 < \chi$.

The solution (2.5.45) diverges logarithmically at $\chi = 1$. Then, to ensure a proper normalization, we need to find a solution (2.5.43) so that the divergent and the constant terms agree as $\chi \to 1^+$ and $\chi \to 1^-$. Then we can interpret the inner product (2.5.35) as a principal value integral so that the contributions of the divergences cancel each other when $\chi \to 1$.

We have the following expansion for the hypergeometric function ${}_2F_1(a, b, a+b, z)$ near $z = 1$:

$$\begin{aligned}{}_2F_1(a, b, a+b, z) = \frac{\Gamma(a+b)}{\Gamma(a)\Gamma(b)}\sum_{n=0}^{\infty}\frac{(a)_n(b)_n}{(n!)^2}\Big(&-\ln(1-z) + 2\psi(n+1) \\ &- \psi(a+n) - \psi(b+n)\Big)(1-z)^n.\end{aligned} \tag{2.5.46}$$

Therefore near $\chi = 1$ the solution $F(\chi)$ for $\chi > 1$, (2.5.45), is given by

$$\begin{aligned}F_\alpha(\chi) &= \frac{\Gamma\left(\frac{1}{2}-\alpha\right)\Gamma(\alpha)}{\sqrt{\pi}}{}_1F_2\left(\alpha, \frac{1}{2}-\alpha, \frac{1}{2}, \frac{(2-\chi)^2}{\chi^2}\right) \\ &= -\ln\left(\frac{(2-\chi)^2}{\chi^2} - 1\right) + 2\psi(1) - \psi(\alpha) - \psi\left(\frac{1}{2}-\alpha\right) + O\left(\frac{(2-\chi)^2}{\chi^2} - 1\right).\end{aligned} \tag{2.5.47}$$

Now we can use the following properties of the digamma function $\psi(z)$:

$$\psi(-z) = \psi(z) + \pi\cot(\pi z) + \frac{1}{z}, \tag{2.5.48}$$

$$\psi(z) = \psi(z+1) - \frac{1}{z}, \tag{2.5.49}$$

$$\psi(z) + \psi\left(z + \frac{1}{2}\right) = 2\psi(2z) - \ln(4), \tag{2.5.50}$$

$$\psi(1) = -\gamma, \tag{2.5.51}$$

to show that

$$2\psi(1) - \psi(\alpha) - \psi\left(\frac{1}{2} - \alpha\right) = -2\gamma - 2\psi(2\alpha) + \pi\tan(\pi\alpha) + \ln(4). \tag{2.5.52}$$

Using the familiar properties of the natural logarithm, it is easy to show that

$$\ln\left(\frac{(2-\chi)^2}{\chi^2} - 1\right) = \ln(\chi - 1) - \ln(x) - \ln\left(\frac{1}{x}\right) + \ln(4). \tag{2.5.53}$$

Substituting these two relations, (2.5.52) and (2.5.53), into the expansion (2.5.47), we find that in the limit $\chi \to 1^+$, we have that

$$F_\alpha(\chi) = -\ln(\chi - 1) + 2\gamma - 2\psi(2\alpha) + \pi\tan(\pi\alpha),\ \chi > 1. \tag{2.5.54}$$

Expanding the general solution to the eigenvalue equation, (2.5.43), similarly, we find that in the $\chi \to 1^-$ limit:

$$\begin{aligned} F_\alpha(\chi) = {} & A\frac{\Gamma(4\alpha)}{\Gamma(2\alpha)^2}\left(-\ln(1-\chi) - 2\gamma - 2\psi(2\alpha)\right) \\ & + B\frac{\Gamma(2-4\alpha)}{\Gamma(1-2\alpha)^2}\left(-\ln(1-\chi) - 2\gamma - 2\psi(2\alpha) - 2\pi\cot(2\pi\alpha)\right),\ \chi < 1 \end{aligned} \tag{2.5.55}$$

It is now easy to see that if we have

$$A = \frac{\Gamma(2\alpha)^2}{2\Gamma(4\alpha)}(1 + \sec(2\pi\alpha)), \tag{2.5.56}$$

$$B = -\frac{\Gamma(1-2\alpha)^2}{2\Gamma(2-4\alpha)}\tan(2\pi\alpha)\tan(\pi\alpha), \tag{2.5.57}$$

then in the limit $\chi \to 1^-$ we have the desired expression for $F_\alpha(\chi)$ when $\chi < 1$

$$F_\alpha(\chi) = -\ln(1-\chi) + 2\gamma - 2\psi(2\alpha) + \pi\tan(\pi\alpha),\ \chi < 1. \tag{2.5.58}$$

Putting all together, we see that we have a following solution for the function $F(\chi)$:

$$F_\alpha(\chi) = \begin{cases} \frac{\Gamma(2\alpha)^2}{2\Gamma(4\alpha)}(1+\sec(2\pi\alpha))\chi^{2\alpha}{}_2F_1(2\alpha,2\alpha,4\alpha,\chi) & \\ -\frac{\Gamma(1-2\alpha)^2}{2\Gamma(2-4\alpha)}\tan(2\pi\alpha)\tan(\pi\alpha)\chi^{1-2\alpha}{}_2F_1(1-2\alpha,1-2\alpha,2-4\alpha,\chi) & 0<\chi<1 \\ \frac{\Gamma\left(\frac{1}{2}-\alpha\right)\Gamma(\alpha)}{\sqrt{\pi}}{}_1F_2\left(\alpha,\frac{1}{2}-\alpha,\frac{1}{2},\frac{(2-\chi)^2}{\chi^2}\right) & 1<\chi \end{cases} \tag{2.5.59}$$

up to the normalization which we will work out below. We still need to ensure that the solution (2.5.59) is normalizable with respect to the inner product (2.5.35). As we will see below, this requires that the function $F(\chi)$ vanishes at least as $F(\chi) \to \chi^{1/2} \to 0$ as $\chi \to 0$. This happens in two cases: One is that $\alpha = 1/4 + is$, $s \in \mathbb{R}$ so that both terms in the $\chi < 1$ solution (2.5.59) are proportional to $\chi^{1/2}$. The other possibility is that $\alpha = n$, $n \in \mathbb{N}$ so that the second term in the $\chi < 1$ solution (2.5.59) vanishes. These two sets of eigenfunctions form a complete basis of normalizable eigenfunctions of the Casimir operator $\mathcal{C}_{1+2}$ and consequently of the kernel $K(t_1,t_2,t_3,t_4)$.

In the case $\alpha = 1/4 + is$, we have an integral representation for the solution $F(\chi)$, which is valid on the whole interval $0 < \chi < \infty$:

$$F_\alpha(\chi) = \frac{1}{2}\int_{-\infty}^{\infty} dy \frac{|\chi|^{2\alpha}}{|y|^{2\alpha}|\chi-y|^{2\alpha}|1-\chi|^{1-2\alpha}}. \tag{2.5.60}$$

Clearly the integral is divergent in the case $\alpha = n$, but $F_\alpha(\chi)$ is its analytical continuation via (2.5.59).

2.5.5 Normalization and the Inner Products for the Eigenfunctions

We still need to work out the normalization of the functions $F_\alpha(\chi)$. We have to analyse the cases $\alpha = 1/4 + is$ and $\alpha = n$ separately. Let us begin with $\alpha = 1/4 + is$:

Let us consider the inner product (2.5.35) of two functions $F_\alpha(\chi)$ and $F_{\alpha'}(\chi)$ with $\alpha = 1/4 + is$ and $\alpha' = 1/4 + is'$. Then we expect that the inner product of these two functions is proportional to $\delta(s - s')$:

$$\langle F_\alpha(\chi), F_{\alpha'}(\chi)\rangle \sim \delta(s - s'). \tag{2.5.61}$$

Based on this expectation, we can consider the integral in the inner product around the point $\chi = 0$, where we can approximate ${}_2F_1(a, b, c, \chi) = 1$ (this relation is exact in the limit $\chi \to 0$). Then the integral around $\chi = 0$ is

$$\begin{aligned} &-\frac{\Gamma(2\alpha)^2}{2\Gamma(4\alpha)}(1+\sec(2\pi\alpha))\frac{\Gamma(1-2\alpha)^2}{2\Gamma(2-4\alpha)}\tan(2\pi\alpha)\tan(\pi\alpha)\int_0^\epsilon \frac{d\chi}{\chi}(\chi^{i(s-s')}+\chi^{-i(s-s')}) \\ &= \frac{\pi\tan(2\pi\alpha)}{8\alpha-2}\int_0^\epsilon \frac{d\chi}{\chi}(\chi^{i(s-s')} + \chi^{-i(s-s')}). \end{aligned} \tag{2.5.62}$$

Making a change of variables $y = \ln(\chi)$, we get

$$= \frac{\pi\tan(2\pi\alpha)}{8\alpha-2}\int_{-\infty}^{\ln(\epsilon)} dy(e^{iy(s-s')} + e^{-iy(s-s')}). \tag{2.5.63}$$

Taking the limit $\epsilon \to 1$ and rearranging, we get

$$= \frac{\pi\tan(2\pi\alpha)}{8\alpha-2}\int_{-\infty}^{\infty} dy e^{iy(s-s')} = \frac{\pi^2\tan(2\pi\alpha)}{4\alpha-1}\delta(s-s'). \tag{2.5.64}$$

We might expect that taking the limit $\epsilon \to 1$ might add some finite terms, since we can no longer approximate ${}_2F_1(a, b, c, \chi) = 1$, and that we would get some finite contributions also from the interval $1 < \chi < 2$. This cannot, however, be the case since we know that the functions $F_\alpha(\chi)$ and $F_{\alpha'}(\chi)$ must be orthogonal for $\alpha \neq \alpha'$ ($s \neq s'$). We cannot get any other contributions proportional to $\delta(s - s')$, since we do not have strong enough divergences at any point but $\chi = 0$. Therefore we deduce that

$$\langle F_\alpha(\chi), F_{\alpha'}(\chi)\rangle = \frac{\pi^2\tan(2\pi\alpha)}{4\alpha-1}\delta(s-s'). \tag{2.5.65}$$

Note that the derivation depended on the fact that in the limit $\chi \to 0$ the functions $F_\alpha(\chi)$ vanished at least as $\chi^{1/2}$. Had this not been the case, we would have had

divergence in the limit $\chi \to 0$ even in the case $s \neq s'$.

The normalization in the case $\alpha = n$ is somewhat similar. It can be shown [14] that in this case we have

$$F_\alpha = 2\mathrm{Re}\left[Q_{\alpha-1}\left(\frac{2-\chi}{\chi}\right)\right], \tag{2.5.66}$$

where Q_n is the Legendre Q function. Substituting this to the inner product (2.5.35) and making a change of variables $y = (2-\chi)/\chi$, we get

$$\langle F_\alpha(\chi), F_{\alpha'}(\chi)\rangle = 2\int_0^\infty Re\left[Q_\alpha(y)\right] Re\left[Q_{\alpha'}(y)\right] = \frac{\pi^2}{8\alpha - 2}\delta_{\alpha\alpha'}. \tag{2.5.67}$$

We still need to calculate the inner product $\langle \Gamma_0(\chi), F_\alpha(\chi)\rangle$, since we need this to expand Γ_0 in terms of the eigenfunctions of the kernel. To do this, we can use the definition of Γ_0 given in (2.5.7) and express this in terms of the cross ratio χ.

$$\begin{aligned}
\Gamma_0(\chi) &= \frac{\Gamma_0(t_1,t_2,t_3,t_4)}{G(t_1,t_2)G(t_3,t_4)} = -\frac{G(t_1,t_3)G(t_2,t_4)}{G(t_1,t_2)G(t_3,t_4)} + \frac{G(t_1,t_4)G(t_2,t_3)}{G(t_1,t_2)G(t_3,t_4)} \\
&= -\mathrm{sgn}\left(\frac{(t_1-t_2)(t_3-t_4)}{(t_1-t_3)(t_2-t_4)}\right)\sqrt{\left|\frac{(t_1-t_2)(t_3-t_4)}{(t_1-t_3)(t_2-t_4)}\right|} \\
&+ \mathrm{sgn}\left(\frac{(t_1-t_2)(t_3-t_4)}{(t_1-t_4)(t_2-t_3)}\right)\sqrt{\left|\frac{(t_1-t_2)(t_3-t_4)}{(t_1-t_4)(t_2-t_3)}\right|} \\
&= \mathrm{sgn}(\chi)\sqrt{|\chi|} + \mathrm{sgn}\left(\frac{\chi}{1-\chi}\right)\sqrt{\left|\frac{\chi}{1-\chi}\right|} \\
&= \begin{cases} \sqrt{\frac{\chi}{1-\chi}} - \sqrt{\chi} & 0 < \chi < 1 \\ -\sqrt{\frac{\chi}{\chi-1}} - \sqrt{\chi} & 1 < \chi < \infty \end{cases}.
\end{aligned} \tag{2.5.68}$$

We have already earlier shown that the function $F_\alpha(\chi)$ has a symmetry

$$F_\alpha(\chi) = F_\alpha\left(\frac{\chi}{1-\chi}\right). \tag{2.5.69}$$

We can then extend $F_\alpha(\chi)$ to the whole real axis by demanding that this symmetry applies for all $\chi \in \mathbb{R}$. We immediately see that this extension is given by the integral representation (2.5.60) and its analytical continuation in the case $\alpha = n$. Using this continuation, let us note the following identity, which follows from a

change of variables $\chi \to \chi/(1-\chi)$ and the symmetry (2.5.69):

$$\int_0^1 \frac{d\chi}{\chi^2} F(\chi)\text{sgn}\left(\frac{\chi}{1-\chi}\right)\sqrt{\frac{\chi}{1-\chi}} = \int_{-\infty}^0 F(\chi)\text{sgn}(\chi)\sqrt{|\chi|}, \tag{2.5.70}$$

and a similar identity, which follows from a change of variables $\chi \to \chi/(\chi-1)$:

$$\int_1^2 \frac{d\chi}{\chi^2} F(\chi)\text{sgn}\left(\frac{\chi}{\chi-1}\right)\sqrt{\frac{\chi}{1-\chi}} = \int_2^\infty F(\chi)\text{sgn}(\chi)\sqrt{|\chi|}. \tag{2.5.71}$$

Using these identities and the expression (2.5.68) for $\Gamma_0(\chi)$, we can express the inner product $\langle F_\alpha(\chi), \Gamma_0\rangle$ as:

$$\begin{aligned}
\langle F_\alpha(\chi), \Gamma_0\rangle &= \int_0^2 \frac{d\chi}{\chi^2} F_\alpha(\chi)^* \Gamma_0(\chi) \\
&= \int_0^2 \frac{d\chi}{\chi^2} F_\alpha(\chi)\text{sgn}(\chi)\sqrt{\chi} + \int_0^1 \frac{d\chi}{\chi^2} F_\alpha(\chi)\text{sgn}\left(\frac{\chi}{1-\chi}\right)\sqrt{\frac{\chi}{1-\chi}} \\
&+ \int_1^2 \frac{d\chi}{\chi^2} F_\alpha(\chi)\text{sgn}\left(\frac{\chi}{1-\chi}\right)\sqrt{\frac{\chi}{1-\chi}} \\
&= \int_{-\infty}^\infty \frac{d\chi}{\chi^2} F_\alpha(\chi)\text{sgn}(\chi)\sqrt{|\chi|}.
\end{aligned} \tag{2.5.72}$$

Finally, using the representation (2.5.60) for $F_\alpha(\chi)$ we find that we can express this as the following double integral:

$$\langle F_\alpha(\chi), \Gamma_0\rangle = \int d\chi dy \frac{\text{sgn}(\chi)}{|\chi|^{2-2\alpha-1/2}|\chi-y|^{2\alpha}|1-y|^{1-2\alpha}|y|^{2\alpha}}. \tag{2.5.73}$$

This is similar to the integrals we encountered in section 2.5.2 and we can use the same methods to compute this integral. Doing this, we find that

$$\langle F_\alpha(\chi), \Gamma_0\rangle = \frac{\pi}{2\alpha - \frac{1}{2}} \tan\left(\pi\left(\frac{1}{4} - \alpha\right)\right). \tag{2.5.74}$$

2.5.6 Eigenvalues of the Kernel

We have thus far shown that the functions $F_\alpha(\chi)$ given by (2.5.59) are the eigenvalues of the differential operator $\mathcal{C}_\chi = (\chi^2 - \chi^3)\partial_\chi^2 - \chi^2\partial_\chi$ with eigenvalues $2\alpha(2\alpha-1)$. We have also shown that the Casimir operator $\mathcal{C}_{1+2}$ defined in (2.5.29) acts on the combination $1/(|t_1-t_2|)^{1/2}F(\chi)$ as follows:

$$\mathcal{C}_{1+2}\frac{1}{\sqrt{|t_1-t_2|}}F_\alpha(\chi) = \frac{1}{\sqrt{|t_1-t_2|}}\mathcal{C}_\chi F_\alpha(\chi), \tag{2.5.75}$$

From this, we immediately see that $G(t_1,t_2)G(t_3,t_4)F(\chi)$ is an eigenfunction of the Casimir operator $\mathcal{C}_{1+2}$ with eigenvalue $2\alpha(2\alpha-1)$ because using the previously proven relations we have that

$$\begin{aligned}\mathcal{C}_{1+2}G(t_1,t_2)G(t_3,t_4)F(\chi) &= \left(\frac{1}{4\pi J^2}\right)^{1/2}\mathcal{C}_{1+2}\frac{\mathrm{sgn}(t_1-t_2)}{\sqrt{|t_1-t_2|}}\frac{\mathrm{sgn}(t_3-t_4)}{\sqrt{|t_3-t_4|}}F_\alpha(\chi)\\ &= \left(\frac{1}{4\pi J^2}\right)^{1/2}\frac{\mathrm{sgn}(t_1-t_2)}{\sqrt{|t_1-t_2|}}\frac{\mathrm{sgn}(t_3-t_4)}{\sqrt{|t_3-t_4|}}\mathcal{C}_\chi F_\alpha(\chi)\\ &= 2\alpha(2\alpha-1)G(t_1,t_2)G(t_3,t_4)F_\alpha(\chi). \end{aligned} \tag{2.5.76}$$

As discussed before, since the kernel $K(t_1,t_2,t_3,t_4)$ commutes with $\mathcal{C}_{1+2}$ in the sense of (2.5.28) the eigenfunctions $G(t_1,t_2)G(t_3,t_4)F_\alpha(\chi)$ must also be eigenfunctions of the kernel. We need still, however, to find the eigenvalues of $G(t_1,t_2)G(t_3,t_4)F_\alpha(\chi)$ when operated on by the kernel instead of the Casimir operator, since these obviously need not be the same. To this end, let us note that using the integral expression (2.5.60) for $F_\alpha(\chi)$, we can write

$$\begin{aligned}G(t_1,t_2)G(t_3,t_4)F_\alpha(\chi) &\sim \frac{\mathrm{sgn}(t_1-t_2)}{\sqrt{|t_1-t_2|}}\frac{\mathrm{sgn}(t_3-t_4)}{\sqrt{|t_3-t_4|}}F_\alpha(\chi)\\ &= \frac{1}{2}\int dt_0 \frac{\mathrm{sgn}(t_1-t_2)}{|t_1-t_0|^{2\alpha}|t_2-t_0|^{2\alpha}|t_1-t_2|^{1/2-2\alpha}}\\ &\times \frac{\mathrm{sgn}(t_3-t_4)}{|t_3-t_0|^{1-2\alpha}|t_4-t_0|^{1-2\alpha}|t_3-t_4|^{2\alpha-1/2}}. \end{aligned} \tag{2.5.77}$$

This is a superposition of functions of the form

$$f_{t_0}(t_t,t_2) = \frac{\mathrm{sgn}(t_1-t_2)}{|t_1-t_0|^{2\alpha}|t_2-t_0|^{2\alpha}|t_1-t_2|^{1/2-2\alpha}}. \tag{2.5.78}$$

Since $G(t_1,t_2)G(t_3,t_4)F_\alpha(\chi)$ is an eigenfunction of $\mathcal{C}_{1+2}$ regardless of the functional form of $G(t_3,t_4)$, we might expect that every function of the form (2.5.78) is separately an eigenfunction of $\mathcal{C}_{1+2}$, regardless of the values of α and t_0. This is indeed true, which is easy to check directly. Furthermore, we deduce that the eigenvalue corresponding to $f_{t_0}(t_1,t_2)$ is independent of t_0 since when operating on it by the kernel $K(t_1,t_2,t_3,t_4)$, we can use the $SL(2)$ symmetry to change the value of t_0 without affecting the eigenvalue. We can exploit this and take $t_0\to\infty$ to get an

eigenfunction of the form

$$f_\infty(t_t, t_2) = \frac{\mathrm{sgn}(t_1 - t_2)}{|t_1 - t_2|^{1/2-2\alpha}}. \tag{2.5.79}$$

This eigenfunction will have the same eigenvalue as $G(t_1, t_2)G(t_3, t_4)F_\alpha(\chi)$. We also notice that this is exactly the same eigenfunction which we guessed based on the form of the kernel in the section 2.5.2. Therefore we can immediately use the result from that section that the eigenvalues corresponding to $f_\infty(t_1, t_2)$ and thus to $G(t_1, t_2)G(t_3, t_4)F_\alpha(\chi)$ when operated on by the kernel are

$$g(\alpha) = \frac{3}{4\alpha - 1} \tan\left(\pi\left(\frac{1}{4} - \alpha\right)\right). \tag{2.5.80}$$

In particular, in the case $\alpha = 1/4 + is$, the eigenvalues are given by

$$g(\alpha) = \frac{3}{4}\frac{\tanh(\pi s)}{s}. \tag{2.5.81}$$

Since $\tanh(x)/x \leq 1$ for all $s \in \mathbb{R}$, the eigenvalues $g(\alpha) < 1$ for all $\alpha = 1/4 + is$. In the case $\alpha = n \in \mathbb{N}$

$$g(\alpha) = \frac{3}{4n - 1} \tan\left(\pi\left(\frac{1}{4} - n\right)\right). \tag{2.5.82}$$

Now we see that $g(\alpha) = 1$ for $n = 1$. This will cause problems when inverting the kernel and we will find that we have to treat the case $\alpha = 1$ using perturbation theory. For $n > 1$ we have that $g(\alpha) < 1$, so the other values of α will not cause any problems.

2.5.7 Sum of the Ladder Diagrams

To calculate the sum of the ladder diagrams, we wanted to diagonalise the kernel. We have now found the eigenfunctions $G(t_1, t_2)G(t_3, t_4)$ of the kernel $K(t_1, t_2, t_3, t_4)$. We have shown that all the ladder diagrams with $n + 1$ rungs can be generated operating on the n-rung ladder diagram by the kernel (see (2.5.5)):

$$\Gamma_{n+1}(t_1, t_2, t_3, t_4) = \int dt_a dt_b K(t_1, t_2, t_a, t_b)\Gamma_n(t_a, t_b, t_3, t_4). \tag{2.5.83}$$

Let us formally write this in a more compact form as

$$\Gamma_{n+1}(t_1,t_2,t_3,t_4) = K(t_1,t_2,t_a,t_b)\Gamma_n(t_a,t_b,t_3,t_4). \tag{2.5.84}$$

Using the same notation, we have that

$$\Gamma_n(t_1,t_2,t_3,t_4) = K(t_1,t_2,t_a,t_b)^n\Gamma_0(t_a,t_b,t_3,t_4). \tag{2.5.85}$$

Therefore the sum of all the ladder diagrams, $\Gamma(t_1,t_2,t_3,t_4)$ is given by

$$\Gamma(t_1,t_2,t_3,t_4) = \sum_n \Gamma_n(t_1,t_2,t_3,t_4) = \sum_n K(t_1,t_2,t_3,t_4)^n\Gamma_0(t_1,t_2,t_3,t_4). \tag{2.5.86}$$

Now we can expand $\Gamma_0(t_1,t_2,t_3,t_4)$ using a complete set of the eigenfunctions of the kernel $G(t_1,t_2)G(t_3,t_4)F(\chi)$, so that we get

$$\begin{aligned}
&K(t_1,t_2,t_3,t_4)^n\Gamma_0(t_1,t_2,t_3,t_4) = K(t_1,t_2,t_3,t_4)^nG(t_1,t_2)G(t_3,t_4)\Gamma_0(\chi)\\
&= \int d\alpha K(t_1,t_2,t_3,t_4)^nG(t_1,t_2)G(t_3,t_4)F_\alpha(\chi)\frac{\langle\Gamma_0(\chi),F_\alpha(\chi)\rangle}{\langle F_\alpha(\chi),F_\alpha(\chi)\rangle}\\
&= \int d\alpha g(\alpha)^nG(t_1,t_2)G(t_3,t_4)F_\alpha(\chi)\frac{\langle\Gamma_0(\chi),F_\alpha(\chi)\rangle}{\langle F_\alpha(\chi),F_\alpha(\chi)\rangle},
\end{aligned} \tag{2.5.87}$$

where we have recalled that we defined earlier $\Gamma_0(\chi) = G(t_1,t_2)^{-1}G(t_3,t_4)^{-1}\Gamma_0(t_1,t_2,t_3,t_4)$ in (2.5.27). The integral over α denotes formally the integral over the continuous set of solutions $F_\alpha(\chi)$ with $\alpha = 1/4 + is$ and the sum over the discrete solutions with $\alpha = n$. Substituting this to the sum of all ladder diagrams (2.5.86), we find that

$$\Gamma(t_1,t_2,t_3,t_4) = \int d\alpha \sum_n g(\alpha)^nG(t_1,t_2)G(t_3,t_4)F(\chi)\frac{\langle\Gamma_0(\chi),F(\chi)\rangle}{\langle F(\chi),F(\chi)\rangle}. \tag{2.5.88}$$

When $|g(\alpha)| < 1$, we can use the formula for the geometric series. In the previous section we showed that the eigenvalues $|g(\alpha)| < 1$ except for the case $\alpha = 1$. Therefore we have that

$$\begin{aligned}
\Gamma(t_1,t_2,t_3,t_4) &= \int_0^\infty ds\frac{1}{1-g(1/4+is)}G(t_1,t_2)G(t_3,t_4)F_\alpha(\chi)\frac{\langle\Gamma_0(\chi),F_\alpha(\chi)\rangle}{\langle F_\alpha(\chi),F_\alpha(\chi)\rangle}\\
&+\sum_{n\neq 1}\frac{1}{1-g(1/4+is)}G(t_1,t_2)G(t_3,t_4)F(\chi)\frac{\langle\Gamma_0(\chi),F_\alpha(\chi)\rangle}{\langle F_\alpha(\chi),F_\alpha(\chi)\rangle}\\
&+\sum_n g(1)^nG(t_1,t_2)G(t_3,t_4)F_\alpha(\chi)\frac{\langle\Gamma_0(\chi),F_\alpha(\chi)\rangle}{\langle F_\alpha(\chi),F_\alpha(\chi)\rangle}.
\end{aligned} \tag{2.5.89}$$

The last term corresponding to the case $\alpha = 1$ appears to diverge, but this is due to the low-energy approximation we made earlier. Without it the $\alpha = 1$ contribution would not diverge. The $\alpha = 1$ contribution can, however, be treated perturbatively so that it gives a finite contribution. We will take a look at this later. For now we just denote this term by $\delta\Gamma$. Substituting in the expressions for $g(\alpha)$, $\langle F_\alpha(\chi)\rangle, \Gamma_0(\chi)$ and $\langle F_\alpha(\chi), F_\alpha(\chi)\rangle$ that we have calculated in the previous sections, we get a following result:

$$\Gamma(t_1,t_2,t_3,t_4) = \frac{8}{\pi}G(t_1,t_2)G(t_3,t_4)\int_0^\infty ds \frac{\tanh(2\pi s)}{4s\coth(\pi s)-3}F_{1/4+is}(\chi)$$
$$+G(t_1,t_2)G(t_3,t_4)\sum_{n\neq 2}\left(\frac{(1-4n)^2\cot(2\pi n)}{\pi^2\left(4n-3\cot\left(\pi\left(n+\frac{1}{4}\right)\right)-1\right)}-\frac{2\pi}{3}\right)F_n(\chi)+\delta\Gamma, \tag{2.5.90}$$

where $\delta\Gamma$ denotes the contribution from the $\alpha = 1$ term.

The calculation of $\delta\Gamma$ is a rather lengthy process and therefore the full calculation is outside the scope of this text, but this calculation has been done in detail in [14]. The basic idea is to study a perturbation of the kernel, δK, on the thermal circle i.e. using the coordinates θ_i given by the transformation below. The kernel on the thermal circle is given by doing a transformation

$$t_i = \tan\left(\frac{\theta_i}{2}\right), \tag{2.5.91}$$

which results in a kernel on the thermal circle given by $K(\theta_1,\theta_2,\theta_3,\theta_4)$. The small expansion parameter in the perturbative expansions can be taken to be $1/(\beta J)$, which was approximated to be zero in the infrared limit.

Then it is possible again find the $SL(2)$ generators that commute with the kernel on the thermal circle and use the Casimir operator corresponding to these generators to find the eigenfunctions of the kernel corresponding to the case $\alpha = 1$. Doing this, it can be shown that the eigenfunctions with eigenvalue 1 of the kernel on the thermal circle are given by

$$F_{1,n}(\theta_1,\theta_2) = \frac{3}{2\pi^2|n|(n^2-1)}\frac{\exp\left(-in\frac{\theta_1+\theta_2}{2}\right)}{\sin\left(\frac{\theta_1-\theta_2}{2}\right)}\left(\frac{\sin\left(n\frac{\theta_1-\theta_2}{2}\right)}{\tan\left(\frac{\theta_1-\theta_2}{2}\right)}-n\cos\left(n\frac{\theta_1-\theta_2}{2}\right)\right),$$

(2.5.92)

for $|n| > 1$, $n \in \mathbb{Z}$. Using these eigenfunctions and the first-order perturbation of the kernel, δK, we can calculate the corrections to the eigenvalues $g(1,n)$ corresponding to the functions $F_{1,n}(\chi)$ defined above. This results in the following expansion:

$$g(1,n) = 1 - \frac{4g'(2)k}{\beta J}|n| + O\left(\frac{1}{(\beta J)^2}\right). \tag{2.5.93}$$

where k is a constant approximatively equal to $k \approx 0.1872$. This leads to the following leading-order contribution to the four-point function:

$$\delta\Gamma(\theta_1,\theta_2,\theta_3,\theta_4) = G(\theta_1,\theta_2)G(\theta_3,\theta_4)\,\frac{3\sqrt{2}}{2\pi+3\pi^2}\,\beta J \sum_{|n|\geq 2}\frac{e^{in/2(\theta_1+\theta_2+\theta_3+\theta_4)}}{n^2(n^2-1)}$$
$$\times\left(\frac{\sin\left(n\frac{\theta_1-\theta_2}{2}\right)}{\tan\left(\frac{\theta_1-\theta_2}{2}\right)} - n\cos\left(n\frac{\theta_1-\theta_2}{2}\right)\right)\left(\frac{\sin\left(n\frac{\theta_3-\theta_4}{2}\right)}{\tan\left(\frac{\theta_3-\theta_4}{2}\right)} - n\cos\left(n\frac{\theta_3-\theta_4}{2}\right)\right). \tag{2.5.94}$$

To be consistent, we would also have to include the corrections of order $1/(\beta J)$ from the perturbations δG of the two-point functions and the contributions of order 1 from the eigenvalue term $1/(1-g(1,n))$. Including both of these would require computing the second-order corrections to the eigenvalues $g(1,n)$, which is very difficult. In [14] it is conjectured that these corrections are given by

$$g(1,n) = 1 - \frac{4\sqrt{2}g'(2)k}{\beta J}|n| 16 g''(2)\left(\frac{k|n|}{\beta J}\right)^2 + O\left(\frac{1}{(\beta J)}^3\right). \tag{2.5.95}$$

Assuming that this is true, we then get the following corrections from the $\alpha = 1$ term:

$$\delta\Gamma(\theta_1,\theta_2,\theta_3,\theta_4) = G(x)G(x')\left(\frac{1}{\sqrt{2}}\beta J - 2(y-y'-\pi/2)\partial_{y-y'} + 2(x-\pi)\partial_x\right.$$
$$\left. + 2(x'-\pi)\partial_{x'}\right)\sum_{|n|\geq 2}\frac{e^{in(y-y')}}{\pi^2 n^2(n^2-1)}\left(\frac{\sin\left(n\frac{x}{2}\right)}{\tan\left(\frac{x}{2}\right)} - n\cos\left(n\frac{x}{2}\right)\right)$$
$$\times\left(\frac{\sin\left(n\frac{x'}{2}\right)}{\tan\left(\frac{x'}{2}\right)} - n\cos\left(n\frac{x'}{2}\right)\right), \tag{2.5.96}$$

where we have denoted that

$$x = \theta_1 - \theta_2, \qquad x' = \theta_3 - \theta_4, \qquad y = \frac{\theta_1-\theta_2}{2}, \qquad y' = \frac{\theta_3-\theta_4}{2}. \tag{2.5.97}$$

3. Generalizations of the SYK Model

In addition to the SYK model with quartic interactions, defined by (2.1.1) or (2.1.2), considered in the previous section, we can also consider a more general case with q-fold couplings [14]. The action for this model is

$$S = \int dt \left(\frac{i}{2} \sum_i \chi_i \frac{d}{dt} \chi_i + \frac{i^{q/2}}{q!} \sum_{i_1, i_2, \ldots, i_q = 1}^{N} J_{i_1 i_2 \ldots i_q} \chi_{i_1} \chi_{i_2} \cdots \chi_{i_q} \right), \tag{3.0.1}$$

which leads to a Hamiltonian:

$$H = \frac{i^{q/2}}{q!} \sum_{i_1, i_2, \ldots, i_q = 1}^{N} J_{i_1 i_2 \ldots i_q} \chi_{i_1} \chi_{i_2} \cdots \chi_{i_q}. \tag{3.0.2}$$

We had to insert a factor of $i^{q/2}$ in order to keep the Hamiltonian Hermitian for all q. The coupling constants are again independent Gaussian random variables with the exception that the coupling constants are antisymmetric for unequal indices so that for example $J_{i_1 i_2 \ldots i_q} = -J_{i_2 i_1 \ldots i_q}$ when $i_1 \neq i_2$. This time it is most convenient to choose the Gaussian distribution so that the couplings have the following disorder averages:

$$\overline{J_{i_1 i_2 \ldots i_q} J_{j_1 j_2 \ldots j_q}} = \frac{J^2 (q-1)!}{N^{q-1}} \delta_{i_1 j_1} \delta_{i_2 j_2} \ldots \delta_{i_q j_q}, \qquad \overline{J_{i_1 i_2 \ldots i_q}} = 0. \tag{3.0.3}$$

3.1 Two-point Function

The two-point function is again given by melonic diagrams in the large N limit $N \to \infty$. The only difference compared to the special case $q = 4$ is that the vertices

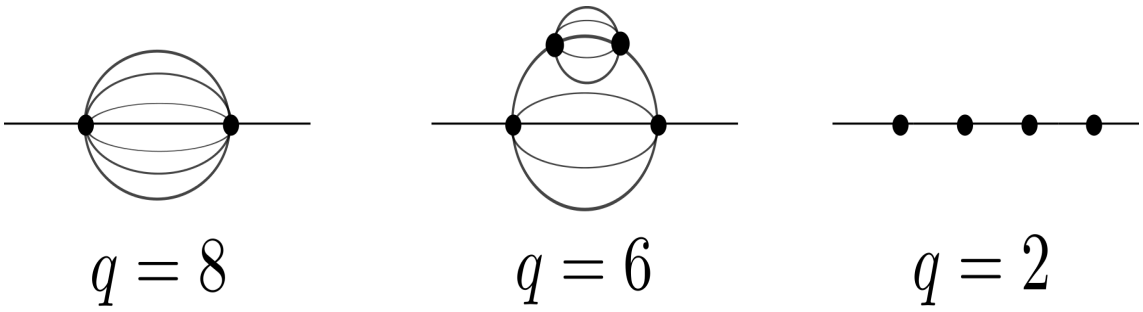

Figure 3.1: *Three examples of melonic diagrams for generalised SYK model. The diagram on the left is for case $q = 8$, the one in the middle for $q = 6$ and the one on the right for $q = 2$.*

are now connected to each other by either 1 or $q - 1$ vertices (see figure 3.1). The proof of this fact is completely similar to the proof we presented for the $q = 4$ special case.

The derivation for the analytical expression of the two-point function in the infrared limit is again very similar to the previous: We can either derive the Schwinger-Dyson equation and solve it or alternatively use the Fourier transform of 2PI to get a following equation

$$G(i\omega)^{-1} = -i\omega - \Sigma(i\omega). \tag{3.1.1}$$

This is exactly the same equation as (2.4.6) except that now

$$\Sigma(t_1, t_2) = J^2 G(t_1, t_2)^{q-1}. \tag{3.1.2}$$

We can use the same trial function, (2.4.19), as before. Doing this, we find that the correct solution to (3.1.1) is

$$G(t_1, t_2) = \left(\frac{\frac{1}{2} - \frac{1}{q}}{J^2 \pi} \tan\left(\frac{\pi}{q}\right) \right)^{1/q} \frac{1}{|t_1 - t_2|^{2/q}} \mathrm{sgn}(t_1 - t_2). \tag{3.1.3}$$

3.1.1 Large q Limit

An interesting feature of the SYK model with q-fold interactions is that the expressions for the two-point function $G(t_1, t_2)$ and the self-energy $\Sigma(t_1, t_2)$ simplify considerably in the large q limit, where we take first $N \to \infty$ and then $q \to \infty$.

Taking the $N \to \infty$ limit gives the results (3.1.2) and (3.1.3). Due to the time translation symmetry of the system, we can without loss of generality take $t_2 = 0$ and $t_1 = t$. Then we can expand $G(t) = G(t, 0)$ and $\Sigma(t) = \Sigma(t, 0)$ as a series in powers of $1/q$ as

$$G(t) = \frac{1}{2}\text{sgn}(t)\left(1 + \frac{1}{q}g(t) + O\left(\frac{1}{q^2}\right)\right), \tag{3.1.4}$$

$$\Sigma(t) = J^2 G(t)^{q-1} = 2^{1-q} J^2 \text{sgn}(t) e^{g(t)}\left(1 + O\left(\frac{1}{q^2}\right)\right), \tag{3.1.5}$$

where $g(t)$ is as yet undetermined function, which will be determined by requiring that the expressions (3.1.4) and (3.1.5) are consistent with the relation (3.1.1), or equivalently with (3.1.2). To do this, we can calculate the Fourier transformation of $G(t)$ up to order $1/q$:

$$G(i\omega) = -i\omega \frac{1}{2q}\mathcal{F}\left[g(t)\text{sgn}(t)\right](i\omega) + O\left(\frac{1}{q^2}\right). \tag{3.1.6}$$

Therefore we have, to the first non-trivial order:

$$\frac{1}{G(i\omega)} = -i\omega + \frac{1}{2q}\omega^2 \mathcal{F}\left[g(t)\text{sgn}(t)\right](i\omega) = -i\omega - \mathcal{F}\left[\frac{1}{2q}\partial_t^2\left(g(t)\text{sgn}(t)\right)\right](i\omega), \tag{3.1.7}$$

where in the last equality we used the properties of the Fourier transform to replace ω with the partial derivative inside the Fourier transformation. Substituting this and (3.1.5) to the equation (3.1.1), we get, to the order $1/q$:

$$\mathcal{F}\left[\frac{1}{2q}\partial_t\left(g(t)\text{sgn}(t)\right)\right](i\omega) = \mathcal{F}\left[2^{1-q} J^2 \text{sgn}(t) e^{g(t)}\right](i\omega). \tag{3.1.8}$$

From this it immediately follows that:

$$\partial_t^2\left(g(t)\text{sgn}(t)\right) = 2^{2-q} q J^2 \text{sgn}(t) e^{g(t)}. \tag{3.1.9}$$

This equation is well-defined in the large q limit if we take the limit $q \to \infty$ so that $2^{2-q}qJ^2$ remains constant. Since the combination qJ^2 is dimensionful, we have always values of t for which the equation (3.1.9) is not well-defined and conversely values for which it is. We are expecting to get such a result that at small time

separations $t \to 0$ the particles behave like free fermions so that $G(t) \to G_0(t)$ as $t \to 0$. We therefore set as a boundary condition that $g(0) = 0$. To completely determine the solution, we also need another boundary condition, which we choose to be of the form $g(a) = 0$.

It is not hard to show that the general solution for (3.1.9) is given by:

$$g(t) = \ln\left(C^2 \frac{2^{q-1}}{J^2 q} \csc(C(|t| + t_0))^2\right), \tag{3.1.10}$$

where C is the constant of integration. Imposing the boundary conditions $g(0) = 0$ and $g(a) = 0$ gives now that [14]

$$g(t) = \ln\left(\left(\frac{\cos\left(\frac{\pi x}{2}\right)}{\cos\left(\pi x\left(\frac{1}{2} - \frac{|t|}{a}\right)\right)}\right)^2\right). \tag{3.1.11}$$

where the constant x can be solved from the equation

$$\frac{x}{\cos\left(\frac{\pi x}{2}\right)} = \sqrt{2^{1-q}q}J\frac{a}{\pi}. \tag{3.1.12}$$

One interesting special case is the limit where $a \to \infty$. Then clearly $x \to 1$. Setting $x = 1$, using (3.1.12) and Taylor expanding the cosine function in the limit $a \to \infty$, we get that:

$$g(t) = -2\ln\left(\sqrt{2^{1-q}q}J|t| + 1\right). \tag{3.1.13}$$

There is also a another, perhaps more intuitive way of arriving at the $q \to \infty$ result for the two-point function [15]. It is based on the observation that due to the symmetry factors the Feynman diagrams that are of the leading non-trivial order in q are those that, if cut vertically in two halves in the middle, would form two tree-level diagram (see figure 3.2a). These diagrams can be more exactly be described as diagrams that can be generated through the following iterative process:

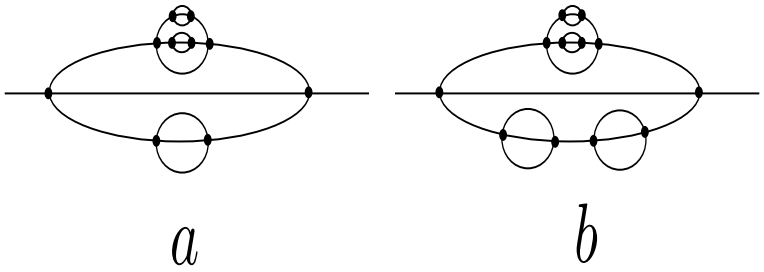

Figure 3.2: *a) Diagram that can be cut into two tree-level diagrams with a single vertical cut. This diagram gives a leading-order contribution in the large q limit. b) Diagram that cannot be cut into two tree-level diagrams with a single vertical cut. This diagram gives a subleading contribution in the large q limit.*

1. Begin with a melonic diagram (figure 3.3a). We call the pair of vertices appearing in a melon each other's pairs.

2. Add a melonic diagram to any line going directly from a vertex to its pair. (figure 3.3b)

3. Repeat from step 2 until the diagram is ripe.

Thus the leading coefficient can be calculated as a sum of all diagrams that can be generate through this iterative process. For the purpose of the following proof we will call such diagrams *simple melonic diagrams*. We will call the original melon a *zeroth-order* melon, any melon placed on a line going from one of its vertices to its pair a *first-order* melon, any melon placed on a line going from a vertex of a second order melon to its pair a *second-order* melon and so on.

We can also form a correspondence between iterated melonic diagrams and tree diagrams illustrated in the figure 3.3. We denote every vertex pair forming a melon by a black node. Then we denote every line going from a vertex to its pair by a white node that is connected to the black node representing the pair of vertices. Every melon that is placed on a line between the vertices is denoted by a new black node that is connected to a white node representing the line. We call nodes corresponding to a zeroth-order melon (both black and white nodes) *zeroth-order* nodes and similarly for higher orders.

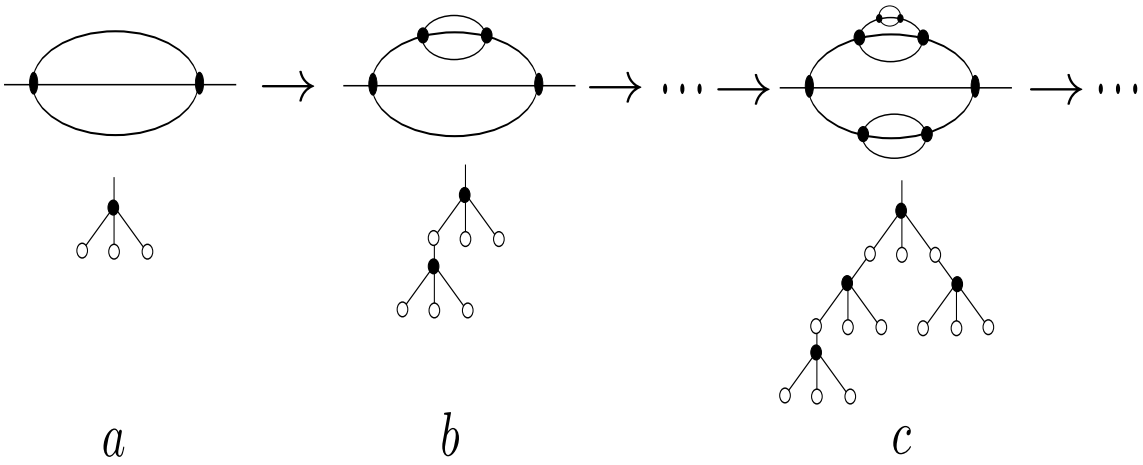

Figure 3.3: *Iterative procedure for creating simple iterated melonic diagrams that can be cut into two tree-level diagrams with a single vertical cut. Below each diagram is its tree diagram representation that we shall use in following proofs. Each pair of vertices corresponds to a single black node and every line between the two vertices is represented as a white node originating from that black node. An iterated melonic diagram is simple if and only if from every white node originates at most one black node.*

Let us now prove that simple melonic diagrams give a contribution that is finite when the limit $q \to \infty$ is taken so that the product qJ^2 is kept constant and that no other diagrams give contribution in this limit.

Theorem 3.1.1. *Simple melonic diagrams give a contribution of order* $1/q$ *in the limit* $q \to \infty$ *so that* qJ^2 *is kept constant.*

Proof. Let us first work out the q dependence of a melon diagram with two vertices. Clearly the two vertices can be connected to each other and two external lines in $q! \times q$ ways. When averaging over the probability distribution the two vertices, due to the way the Gaussian ensemble was defined, give a contribution of

$$\frac{J^2(q-1)!}{N^{q-1}}. \tag{3.1.14}$$

The prefactors from the interaction Hamiltonian gives a factor of $1/q!^2$. The factor of $1/2!$ from the exponential of the Hamiltonian cancels exactly with the factor of 2 that comes from exchanging the two vertices with each other. Finally, summing over the $q-1$ free indices gives a contribution of N^{q-1}. Therefore a melon diagram gives

a contribution of J^2. This result clearly holds if the melonic diagram is connected to other vertices instead of external lines. We need only a slight modification to the argument: now the factor from expanding the exponential of the ineraction Hamiltonian, giving the vertices, cancels the multiplicity factor coming from exchanging any vertices of the full diagram with each other.

We can now show that any simple melonic diagram created by the iterative procedure detailed above has a finite limit when $q \to \infty$ so that qJ^2 is kept constant. To do this, we can consider a simple melonic diagram with n_1 first-order melons, n_2 second order melons and so on. Let us denote $\sum_{k=1}^{\infty} n_k + 1 = n$. We can then show that we get a contribution of

$$q^{n-1} J^{2n} \sim \frac{1}{q}. \tag{3.1.15}$$

First, let us note that since we are taking the $q \to \infty$ limit, we can without loss of generality take $q - 1 > n$. Then we see that we can place the n_1 first-order melons to the $q - 1$ lines between the two vertices of the zeroth-order melon in $(q-1)(q-2)\dots(q-n_1-1)$ ways. (We distinguish different melons and there cannot be more than one melon per line since the diagram is simple. The condition $q - 1 > n$ guarantees that there are more lines than melons, so we do not have to worry about choosing which melons go on the same line.) As shown above, every melon itself gives a contribution of J^2, the diagram where we have placed the first-order melons gives a contribution of

$$(q-1)(q-2)\dots(q-n_1-1)J^{2(n_1+1)}. \tag{3.1.16}$$

In the limit $g \to \infty$, we can disregard every term apart from the leading term, so we get a leading-order contribution of

$$q^{n_1} J^{2(n_1+1)}. \tag{3.1.17}$$

Next, we can place the second-order melons. The exact number of different ways they can be placed depends on how many melons must be placed on lines between the two vertices of each first-order melon. Let us therefore suppose that there are k_0

first-order melons with zero second-order melons placed in between the vertices, k_1 first order melons with one melon placed between the vertices and so on. We must clearly have that:

$$\sum_m k_m = n_1 \text{ and } \sum_m m k_m = n_2. \tag{3.1.18}$$

Then we can choose how many melons we put between each pair of vertices in $\prod_i k_i$ ways. The number of possible combinations gives just a finite constant. Then we can place the k_1 melons in $(q-1)^{k_1}$ ways on the lines in the first-order melons, since we can choose any of the $q-1$ vertices between the two vertices for every melon, because every second-order melon is placed to a separate first-order melon. Similarly, the $2k_2$ melons can be placed in $(q-1)^{k_2}(q-2)^{k_2}$ ways the $3k_3$ melons in $(q-1)^{k_3}(q-2)^{k_3}(q-3)^{k_3}$. Every melon also gives a contribution of J^2 as before. In general the mk_m second-order melons give a contribution of

$$\prod_m^\infty \left(\frac{(q-1)!}{(q-m-1)!}\right)^{k_m} J^{2k_m}. \tag{3.1.19}$$

ways. Then clearly this clearly gives a leading-order contribution proportional to q^{mk_m}. Multiplying all terms discussed previously, we find that placing the second-order melons gives a new factor of

$$q^{\sum_m mk_m} J^{2\sum_m mk_m} \prod_m k_m = C q^{n_2} J^{2n_2}, \tag{3.1.20}$$

where C is a finite constant.

It is now easy to see that a completely similar proof applies to any higher order melons as well. The only difference is in the prefactor, but it is always finite, so it does not affect the powers of q we are interested in. Formally, we could prove by induction that mth-order melons give a factor of

$$C q^{n_m} J^{2n_m}. \tag{3.1.21}$$

Combining the contributions of melons of every order, we then find that our simple iterated melonic diagram gives a leading-order contribution of

$$C J^2 \prod_{m=1}^\infty q^{n_m} J^{2n_m} = C q^{\sum_{m=1}^\infty n_m} J^{2\sum_{m=1}^\infty n_m + 2} = C q^{n-1} J^{2n}, \tag{3.1.22}$$

where the first factor of J^2 is due to the zeroth-order melon and C is again a finite constant. Now we can finally note that in the limit where $q \to \infty$ so that qJ^2 is kept constant, we have

$$Cq^{n-1}J^{2n} = (qJ^2)^{n-1}J^2 \sim \frac{1}{q}. \tag{3.1.23}$$

This finishes the proof. □

After the previous proof it is not hard to prove the following theorem:

Theorem 3.1.2. *Diagrams other than the simple melonic diagrams give a subleading contribution in the large q limit.*

Proof. Let us now consider the representation of the melonic diagrams in terms of tree diagrams as in the figure 3.3. Clearly, an iterated melonic diagram is simple if and only if from every white node originates at most one black node. Thus we need to only prove that any diagram where there are two or more black nodes originating from a single white node gives a subleading contribution.

Let us now consider a diagram with n melons and a white node such that there are at least two black nodes originating from it. Let us assume that the two black nodes originate from an m:th level node. We can then calculate in how many ways the subdiagram whose root is the second black node can be placed in the tree diagram so that it will still correspond to the same diagram if different nodes are not distinguished. It is easy to see that the second black node can only be added to a white node that has a similar subdiagram originating from it as the node to which the black node was originally connected. Since the white node to the black node was originally connected has at least two black nodes connected to it and every black node correspond to a melon, there can be at most n of similar vertices. Then the black node can be connected to the tree diagram only in less than n ways, so it gives a contribution of order zero. This proves that every black node that is connected to the same white node with another black node will give a contribution of order zero.

In previous proof it was shown that if a black node is connected to a white node with no other black nodes, it will give a contribution of order q and the zeroth-order melon (black node) will also give a contribution of order zero. Therefore we can immediately deduce that a diagram with n melons and m black nodes that are connected to a node with at least one other black node can give a contribution of at most

$$Cq^{n-1-m/2}J^{2n} = C(qJ^2)^{n-1-m/2}J^{2+m} \sim \frac{1}{q^m} \tag{3.1.24}$$

This is clearly subleading for $m \neq 0$. This proves the theorem. □

The two proofs above establish that only the simple melonic diagrams contribute in the large q limit. We can form a simple recursion relation for the sum of all melonic diagrams (figure 3.4). The quantity $\Delta(t_1, t_2)$, the sum of all simple melonic diagrams, defined in figure 3.4, has a simple relation to the self-energy in the large q limit. $\Delta(t_1, t_2)$ clearly contains every diagram contributing to $\Gamma(t_1, t_2)$, but contains also an additional free propagator $G_0(t_1, t_2)$. Therefore we can express the self-energy as:

$$\Sigma(t_1, t_2) = \Delta(t_1, t_2) - G_0(t_1, t_2) \tag{3.1.25}$$

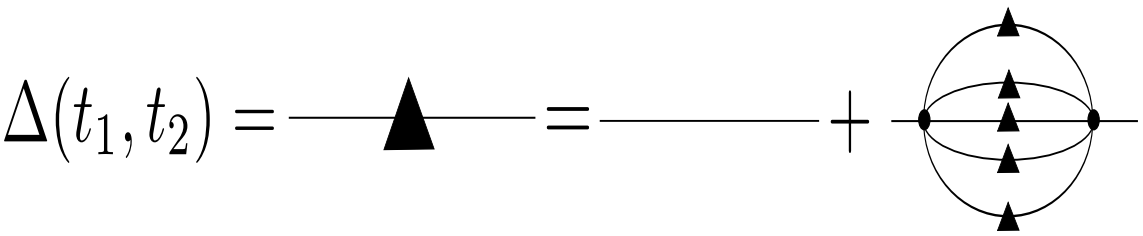

Figure 3.4: *Recursion relation for generating all simple melonic diagrams. The diagrams generated by this recursion are clearly the diagrams contributing to the self-energy $\Sigma(t_1, t_2)$ plus the free propagator $G_0(t_1, t_2)$.*

For the sum of all simple melonic diagrams, we have the following recursion relation:

$$\Delta(t_1, t_2) = G_0(t_1, t_2) + J^2 \left(G_0(t_1, t)\Delta(t, t')G_0(t', t_2)\right)^{q-1}. \tag{3.1.26}$$

Expressing the second term on the right-hand side in terms of the Fourier transformations (setting $t_1 = t$ and $t_2 = 0$ as before), we get that

$$\Delta(t) = G_0(t) + J^2 \left(\int \frac{d\omega}{2\pi} e^{i\omega t} G_0(i\omega)^2 \Delta(i\omega) \right)^{q-1}. \tag{3.1.27}$$

Substituting the expression (2.4.7) for the Fourier transformation of the free 2-point function, $G_0(i\omega)$, and rearranging, we find that

$$\left(\frac{1}{J^2}\Sigma(t) - \frac{1}{J^2} G_0(t) \right)^{1/(q-1)} = - \int \frac{d\omega}{2\pi} e^{i\omega t} \frac{1}{\omega^2} \Delta(i\omega). \tag{3.1.28}$$

Taking the Fourier transformation of this and solving for $\Sigma(i\omega)$, we get a following solution:

$$- \int dt e^{i\omega t} \omega^2 \left(\frac{1}{J^2}\Delta(t) - \frac{1}{J^2} G_0(t) \right)^{1/(q-1)} = \Delta(i\omega). \tag{3.1.29}$$

Using the properties of the Fourier transformation, we can change the factors of ω to derivatives with respect to t. Then taking the inverse Fourier transformation gives:

$$\partial_t^2 \left(\frac{1}{J^2}\Delta(t) - \frac{1}{J^2} G_0(t) \right)^{1/(q-1)} = \Delta(t). \tag{3.1.30}$$

Now, defining, as in (3.1.5), $g(t)$ so that

$$\Sigma(t) = \Delta(t) - G_0(t) = 2^{1-q} J^2 \mathrm{sgn}(t) e^{g(t)}, \tag{3.1.31}$$

and substituting this to (3.1.30), we get the following differential equation for the self-enegry $\Sigma(t) = \Sigma(t, 0)$:

$$\partial_t^2 \left(2^{1-q} J^2 \mathrm{sgn}(t) e^{g(t)} \right)^{1/(q-1)} = 2^{1-q} J^2 \mathrm{sgn}(t) e^{g(t)} + G_0(t). \tag{3.1.32}$$

Simplifying, and keeping only the terms that contribute in the $q \to \infty$ limit, where $2^{2-q} q J^2$ is kept fixed, we find the following equation

$$\partial_t^2 \left(g(t) \mathrm{sgn}(t) \right) = 2^{2-q} q J^2 \mathrm{sgn}(t) e^{g(t)}, \tag{3.1.33}$$

which is exactly the equation (3.1.9) derived before.

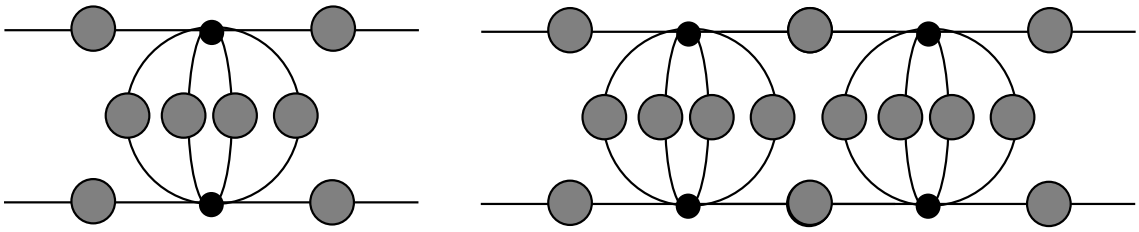

Figure 3.5: *Two examples of ladder diagrams in the case of $q = 6$ theory.*

3.1.2 q=2

Besides the limiting case of $q \to \infty$, there is another exactly solvable case, which is $q = 2$. In this case the self-energy $\Sigma(t)$ is, apart from a constant prefactor, just the two-point function (see figure 3.1):

$$\Sigma(t) = J^2 G(t)^{q-1} = J^2 G(t). \tag{3.1.34}$$

Substituting this to (3.1.1) gives a quadratic equation:

$$\frac{1}{G(i\omega)} = -i\omega - J^2 G(i\omega), \tag{3.1.35}$$

from which we can immediately solve for $G(i\omega)$:

$$G(i\omega) = -i\frac{\omega + \mathrm{sgn}(\omega)\sqrt{4J^2 + \omega}}{2J^2}. \tag{3.1.36}$$

3.2 Four-point Function

The leading contribution to the four-point function in the generalised SYK model consists again of ladder diagrams, as is easy to prove using the same ideas as in the proofs of theorems (2.3.2) and (2.3.1). The only difference to the $q = 4$ case is that the rungs of ladder diagrams have $q - 2$ propagators instead of four (see figure 3.5). Following the logic of section 2.5, we see that the kernel for arbitrary q is given by:

$$K(t_3, t_4, t_a, t_b) \equiv -3J^2 G(t_a, t_3) G(t_b, t_4) G(t_3, t_4)^{q-2}. \tag{3.2.1}$$

In this case, we can consider the generators of the $SL(2)$ algebra of the form:

$$D_i = -t_i \partial_{t_i} - \frac{1}{q}, \qquad P_i = \partial_{t_i}, \qquad K = t_i^2 \partial_{t_i} + \frac{2}{q}. \tag{3.2.2}$$

We again find that these satisfy the "commutation relations" (2.5.23)-(2.5.25) with the kernel $K(t_1, t_2, t_3, t_4)$. Therefore we can again deduce that the following "commutation relation" is true

$$\mathcal{C}_{1+2}K(t_1, t_2, t_3, t_4) = K(t_1, t_2, t_3, t_4)\mathcal{C}_{3+4}, \tag{3.2.3}$$

where $\mathcal{C}_{i+j}$ is defined analogously to the $q = 4$ case, which gives that

$$\mathcal{C}_{i+j} = 2\left(\frac{1}{q^2} - \frac{1}{q}\right) + 2D_iD_j - P_iK_j - K_iP_j. \tag{3.2.4}$$

Apart from the form of the two-point functions, the eigenfunction of this Casimir operator is the same as in the $q = 4$ case, so the eigenfunctions are

$$G(t_1, t_2)G(t_3, t_4)F_\alpha(\chi), \tag{3.2.5}$$

where

$$F_\alpha(\chi) = \begin{cases} \frac{\Gamma(2\alpha)^2}{2\Gamma(4\alpha)}(1 + \sec(2\pi\alpha))\chi^{2\alpha}{}_2F_1(2\alpha, 2\alpha, 4\alpha, \chi) & \\ -\frac{\Gamma(1-2\alpha)^2}{2\Gamma(2-4\alpha)}\tan(2\pi\alpha)\tan(\pi\alpha)\chi^{1-2\alpha}{}_2F_1(1-2\alpha, 1-2\alpha, 2-4\alpha, \chi) & 0 < \chi < 1 \\ \frac{\Gamma\left(\frac{1}{2}-\alpha\right)\Gamma(\alpha)}{\sqrt{\pi}}{}_1F_2\left(\alpha, \frac{1}{2}-\alpha, \frac{1}{2}, \frac{(2-\chi)^2}{\chi^2}\right) & 1 < \chi \end{cases} \tag{3.2.6}$$

The complete set of eigenvectors is again given by two cases of values of α. Either $\alpha = 1/4 + is$ or $\alpha = n$. The continuum eigenfunctions have (up to constant prefactors) the following integral representation

$$\begin{aligned} &G(t_1, t_2)G(t_3, t_4)F_\alpha(\chi) \sim \frac{\mathrm{sgn}(t_1 - t_2)}{|t_1 - t_2|^{2/q}}\frac{\mathrm{sgn}(t_3 - t_4)}{|t_3 - t_4|^{2/q}}F_\alpha(\chi) \\ &= \frac{1}{2}\int dt_0 \frac{\mathrm{sgn}(t_1 - t_2)}{|t_1 - t_0|^{2\alpha}|t_2 - t_0|^{2\alpha}|t_1 - t_2|^{2/q-2\alpha}} \\ &\times \frac{\mathrm{sgn}(t_3 - t_4)}{|t_3 - t_0|^{1-2\alpha}|t_4 - t_0|^{1-2\alpha}|t_3 - t_4|^{2\alpha+2/q-1}}. \end{aligned} \tag{3.2.7}$$

It is easy to verify that the functions of the form

$$f_{t_0}(t_1, t_2) = \frac{\mathrm{sgn}(t_1 - t_2)}{|t_1 - t_0|^{2\alpha}|t_2 - t_0|^{2\alpha}|t_1 - t_2|^{2/q-2\alpha}}. \tag{3.2.8}$$

are eigenfunctions of the Casimir operator $\mathcal{C}_{1+2}$ with any value of t_0, and thus those of the kernel as well. As before, the eigenvalues are independent of t_0. The integral

for calculating the eigenvalues is completely similar to that from the section 2.5.2. Doing the integrals we find the following eigenvalues

$$g(\alpha) = -(q-1)\frac{\Gamma\left(\frac{3}{2}-\frac{1}{q}\right)\Gamma\left(1-\frac{1}{q}\right)\Gamma\left(\frac{1}{q}-\alpha\right)\Gamma\left(\frac{1}{2}+\frac{1}{q}-\alpha\right)}{\Gamma\left(\frac{1}{2}+\frac{1}{q}\right)\Gamma\left(\frac{1}{q}\right)\Gamma\left(\frac{3}{2}-\frac{1}{q}-\alpha\right)\Gamma\left(1-\frac{1}{q}+\alpha\right)}. \tag{3.2.9}$$

From this form it is trivial to show that also in the general q case we have that $\alpha = 1$ gives an eigenvalue of $g(1) = 1$ and therefore we have to treat the $\alpha = 1$ contribution perturbatively also in the general case.

The four-point function is given by very similar expression as in the $q = 4$ case. The only difference is in the eigenvalues $g(\alpha)$ and the inner product $\langle F(\chi), \Gamma_0(\chi)\rangle$:

$$\begin{aligned}\Gamma(t_1,t_2,t_3,t_4) &= \frac{2\pi q}{(q-1)(q-2)\tan(q/\pi)}G(t_1,t_2)G(t_3,t_4)\int_0^\infty ds\frac{4\alpha-1}{2\pi^2\tan(2\pi\alpha)}\\ &\times\frac{g(1/4+is)}{1-g(1/4+is)}F_{1/4+is}(\chi) + G(t_1,t_2)G(t_3,t_4)\frac{2\pi q}{(q-1)(q-2)\tan(q/\pi)}\\ &\times\sum_{n\neq 2}\frac{4\alpha-1}{\pi^2}\frac{g(n)}{1-g(n)}F_n(\chi) + \delta\Gamma.\end{aligned} \tag{3.2.10}$$

The leading-order contribution to the four-point function is given by:

$$\begin{aligned}\delta\Gamma(\theta_1,\theta_2,\theta_3,\theta_4) &= G(\theta_1,\theta_2)G(\theta_3,\theta_4)\,\frac{3\times 2^{(5-q)/2}\sqrt{q}}{\pi k(q)g'(2)(2-3q+q^2)\tan(\pi/q)}\,\beta J\\ &\times\sum_{|n|\geq 2}\frac{e^{in/2(\theta_1+\theta_2+\theta_3+\theta_4)}}{n^2(n^2-1)}\left(\frac{\sin\left(n\frac{\theta_1-\theta_2}{2}\right)}{\tan\left(\frac{\theta_1-\theta_2}{2}\right)} - n\cos\left(n\frac{\theta_1-\theta_2}{2}\right)\right)\\ &\times\left(\frac{\sin\left(n\frac{\theta_3-\theta_4}{2}\right)}{\tan\left(\frac{\theta_3-\theta_4}{2}\right)} - n\cos\left(n\frac{\theta_3-\theta_4}{2}\right)\right),\end{aligned} \tag{3.2.11}$$

where $k(q)$ is a q dependent constant that behaves as $2/q$ for large q [14].

In the $q\to\infty$ case it can be shown that the eigenvalue $g(1)$ gets a following corrections up to the second order, unlike previously where this form was only conjectured:

$$g(1,n) = 1 - \frac{2^{(q+1)/2}g'(2)}{\sqrt{q}\beta J}|n| + \frac{g''(2)}{2}\left(\frac{2^{(q+1)/2}}{\sqrt{q}\beta J}\right)^2 + O(1/(\beta J)^3). \tag{3.2.12}$$

The four-point function for the $q\to\infty$ model is then given, up to order $1/(\beta J)^0$

and $1/q^0$, by

$$\Gamma(\theta_1,\theta_2,\theta_3,\theta_4) = G(x)G(x')\Bigg(\frac{\sqrt{q}}{2^{(q-1)/2}}\beta J - 2(y-y'-\pi/2)\partial_{y-y'} + 2(x-\pi)\delta_x + 2(x'-\pi)\delta_{x'}\Bigg)\sum_{|n|\geq 2}\frac{e^{in(y-y')}}{\pi^2 n^2(n^2-1)}\left(\frac{\sin\left(n\frac{x}{2}\right)}{\tan\left(\frac{x}{2}\right)} - n\cos\left(n\frac{x}{2}\right)\right) \times \left(\frac{\sin\left(n\frac{x'}{2}\right)}{\tan\left(\frac{x'}{2}\right)} - n\cos\left(n\frac{x'}{2}\right)\right), \tag{3.2.13}$$

where again

$$x = \theta_1 - \theta_2, \qquad x' = \theta_3 - \theta_4, \qquad y = \frac{\theta_1-\theta_2}{2}, \qquad y' = \frac{\theta_3-\theta_4}{2}. \tag{3.2.14}$$

4. An SYK-like Model Without Disorder

4.1 Introduction

The SYK model and its generalizations introduced in previous sections 2.1 and 3 have many interesting properties: They are exactly solvable in the large N limit, have conformal symmetry at large energies, have maximally chaotic behaviour and exhibit behaviour expected of dual to an emergent $1+1$ dimensional spacetime. Many of these properties depend on the form of the leading-order Feynman diagrams in the large N expansion. For the SYK model, these were either iterated melonic diagrams in the case of the two-point function or ladder diagrams in the case of the four-point function.

In section 2.3 we presented a proof for the fact that the leading-order diagrams in the large N expansion are indeed melonic diagrams and every melonic diagram is of the leading order. The crucial property of the SYK model which allowed this proof was the fact that the coupling constants $J_{i_1,\ldots,i_q}$ are independent (up to antisymmetry properties) random variables drawn from a Gaussian distribution. This leads to the following expression for the disorder averages:

$$\overline{J_{i_1 i_2 \ldots i_q} J_{j_1 j_2 \ldots j_q}} = \frac{J^2 (q-1)!}{N^{q-1}} \delta_{i_1 j_1} \delta_{i_2 j_2} \ldots \delta_{i_q j_q}, \qquad \overline{J_{i_1 i_2 \ldots i_q}} = 0. \tag{4.1.1}$$

In terms of the Feynman diagrams, this means that every vertex with free indices (colours) $i_1, .., i_q$ must have a corresponding pair with the same free indices (colours)

in order for the diagram to make a non-vanishing contribution. Therefore the random nature of the interactions is essential for the SYK model to have the interesting properties discussed in previous sections. True quantum systems, however, do not have random interactions that are then averaged over disorder. Therefore it is not immediately clear if the SYK model can be used to investigate subtler properties of black holes [9].

This immediately raises the question whether most, if not all, of the properties mentioned before could be exhibited by a more traditional model without disorder. One suggested approach is to replace coupling constants $J_{i_1,..,i_q}$ with fields with extremely slow dynamics [2, 14]. This method would have, however, undesirable consequences: the thermodynamic entropy of the field replacing the couplings $J_{i_1,..,i_q}$ would then be much greater than the entropy of the original fermionic fields χ_i [9].

More recently, Witten [9], building on the work of Gurau and collaborators [10, 11, 12], has proposed a tensor model whose leading-order diagrams for the two-point and four-point functions are the iterated melonic and ladder diagrams, respectively [9, 16]. As a consequence, the two-point function and the four-point function for Witten's tensor model have the same form as their counterparts in the case of SYK model [16].

The model proposed by Witten consists of $q = D+1$ real fermion fields ψ_i, each with n^D components, so that the total number of real fermionic fields is $N = (D+1)n^D$. Every fermion field ψ_i will then have D indices, taking values $0, \ldots, n$, each of which will be contracted with other D fields. Now for every unordered pair of fields ψ_a and ψ_b (or equivalently for every unordered pair of indices from the set $\{0, 1, ..., D\}$, we define a group G_{ab} as a copy of $O(n)$ that acts on the indices that ψ_a and ψ_b are contracted by. For example the contraction $\psi_0^{ijk}\psi_1^{ilm}$ transforms under G_{01}^{xy} (the

upper indices here are exceptionally the matrix indices) as

$$\psi_0^{ijk}\psi_1^{ilm} \to \psi_0^{ijk}G_{01}^{is}\psi_1^{slm} = O^{ip}\psi_0^{pjk}O^{is}\psi_1^{slm} = (O^T)^{pi}\psi_0^{pjk}O^{is}\psi_1^{slm}$$
$$= \psi_0^{pjk}(OO^T)^{ps}\psi_1^{slm} = \psi_0^{pjk}\delta^{ps}\psi_1^{slm} = \psi_0^{pjk}\psi_1^{plm} = \psi_0^{ijk}\psi_1^{ilm}, \tag{4.1.2}$$

where $O \in O(n)$. Therefore the symmetry group of the model is, up to a discrete quotient group

$$G_0 \equiv \prod_{a<b} G_{ab} \cong O(n)^{D(D+1)/2}, \tag{4.1.3}$$

where the product is taken over only pairs with $a < b$ since we do not distinguish the group G_{ab} from G_{ba}. The discrete quontient group that acts trivially on all fields ψ_i can be found by considering the centre of $O(n)$, which is $\mathbb{Z}_2$. Therefore the center of the group G_0 must be $\mathbb{Z}_2^{D(D+1)/2}$. The subgroup of G_0 acting trivially on all ψ_i is a subgroup of $\mathbb{Z}_2^{D(D+1)/2}$, more specifically $\mathbb{Z}_2^{(D-2)(D+1)/2}$. Therefore the full faithfully acting symmetry group of the theory is

$$G \equiv G_0/\mathbb{Z}^{(D-2)(D+1)/2} \cong O(n)^{D(D+1)/2}/\mathbb{Z}^{(D-2)(D+1)/2}. \tag{4.1.4}$$

We can now define an action with this symmetry:

$$S = \int dt \left(\frac{i}{2}\sum_i \psi_i^{j_1\ldots j_D}\frac{d}{dt}\psi_i^{j_1\ldots j_D} - i^{q/2}J\psi_0^{a_1a_2\ldots a_D}\psi_1^{a_1b_2\ldots b_D}\ldots\psi_{D+1}^{\ldots b_{D-1}a_D} \right), \tag{4.1.5}$$

where the upper indices of the second expression are contracted to form a G-invariant expression as described before. This action follows from a Hamiltonian:

$$H = i^{q/2}J\psi_0^{a_1a_2\ldots a_D}\psi_1^{a_1b_2\ldots b_D}\ldots\psi_{D+1}^{\ldots b_{D-1}a_D}. \tag{4.1.6}$$

In the following discussion we concentrate on the special case given by the following Hamiltonian for clarity:

$$H = J\psi^{a_1a_2a_3}\psi^{a_1b_2b_3}\psi^{c_1a_2b_3}\psi^{c_1b_2a_3}. \tag{4.1.7}$$

The generalization to other cases is rather straightforward.

We will next discuss the Feynman diagrams for this theory and present proof that the $1/N$ expansion for this model is dominated by iterated melonic diagrams, following closely [16] and [17].

4.2 Feynman Diagrams

As was the case with the SYK model, it is again useful to use colours to represent different indices. This time we denote different tensor indices with different colours. Thus for example, we get the following expression for the free propagator $\langle \psi^{abc}\psi^{efg}\rangle = \delta^{ae}\delta^{bf}\delta^{cg}$ (figure 4.1).

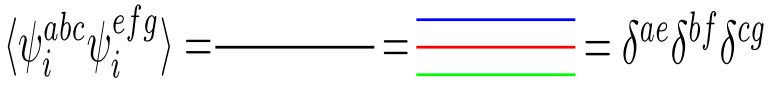

Figure 4.1: *The free propagator of the tensor model represented by two equivalent diagrams. The coloured lines in the second diagram represent the three indices of the tensor fields.*

Looking at the form of the Hamiltonian (4.1.7), we see that every vertex has four incoming lines which can be separated into three lines of different colours. Thus we can express a vertex in four equivalent ways (figure 4.2).

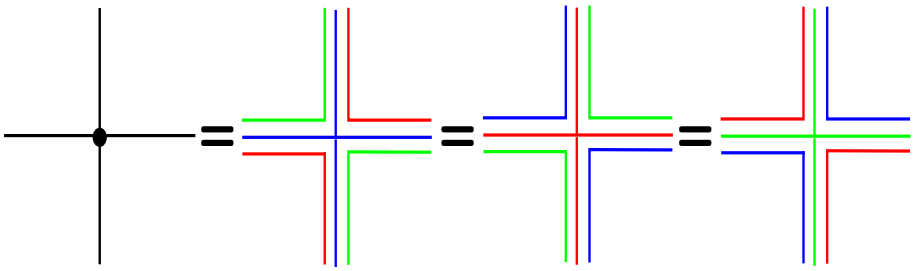

Figure 4.2: *Four equivalent ways of representing a vertex in the tensor theory. The first vertex is just the traditional way of representing a vertex. In the next three vertices we have represented different indices by different colours. Here the blue colour represents the first index, red the second and green the third. All three choices of colours for the middle line are equivalent and the choice does not need to be the same for every vertex in a diagram but every line must be connected to another line of the same colour in order to get a nonzero contribution from the diagram.*

Note that unlike in the case of SYK Feynman rules for coloured diagrams, here the colours do not denote the different free indices but the positions of the index. Below 4.3 we show also a colouring which corresponds to that of the SYK model i.e. every colour corresponds to one free index.

In figures 4.1 and 4.2 different colours correspond to the different placements of the indices. Another way of representing the vertices uses defferent colour for every

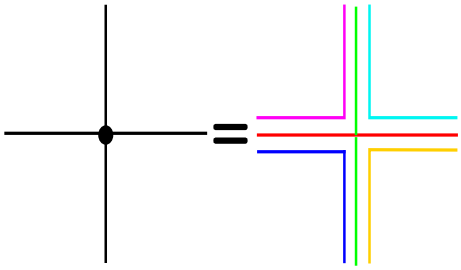

Figure 4.3: *Another way of representing a vertex. Here every colour represents a different free index. In the following we use both representations. It is clear from context which one we are using.*

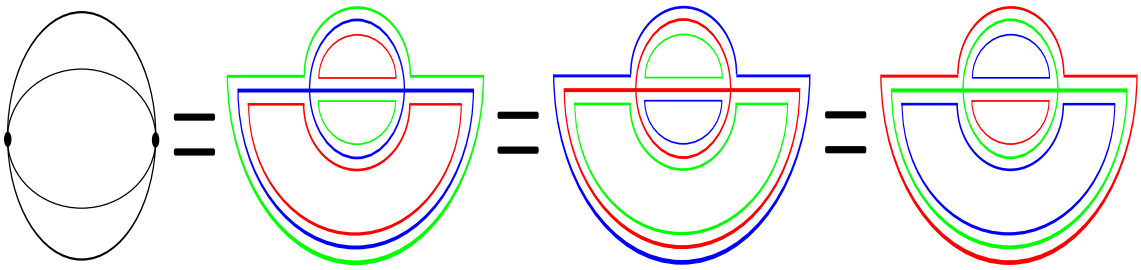

Figure 4.4: *Melonic vacuum graph. Here we are using the representation* (4.2) *for the vertices and lines. As with vertices, there are three equivalent ways of representing this graph with coloured lines, which shows the index structure explicitly. Note that the coloured graphs on the right are still the same as the uncoloured graph even though they have been deformed for illustrative purposes.*

index (see figure 4.3). This is similar to the colouring convention we used for the SYK model.

In figure 4.2, we can also leave the middle lines out so that we get a vertex similar to those of the standard matrix models [16]. The Feynman diagrams with double-line vertices of this kind are called the fat subgraphs of the original three-line graph (figures 4.4 and 4.5).

4.3 Melonic Dominance in the Large N Limit

Let us now concentrate on the vacuum diagrams and prove that the iterated melonic diagrams dominate the large N expansion for the tensor model. To make the connection to the SYK model more explicit, let the indices now take values $0, \ldots, N$.

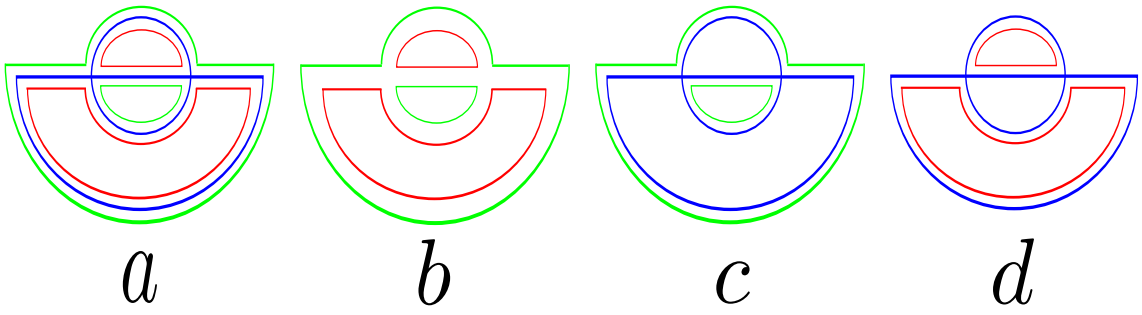

Figure 4.5: *Full melonic vacuum graph (a) and all its fat subgraphs (b,c,d), which can be created by repressing the lines of one colour.*

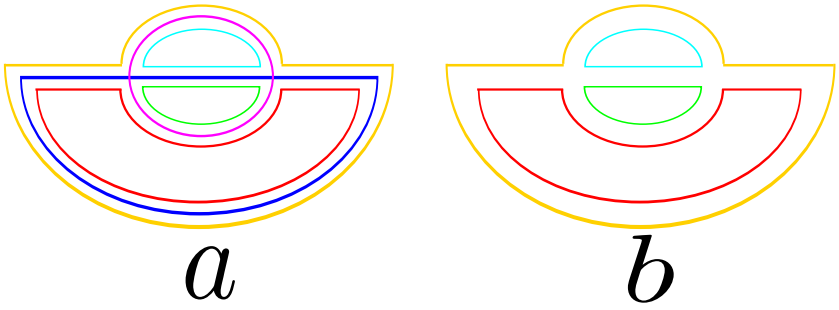

Figure 4.6: *a) Melonic diagram using the colouring convention of figure 4.3 showing every free index in different colour.*

b) Fat subgraph corresponding to the one in the figure 4.5b showing every free index in different colour.

The definition of an iterated melonic diagrams is essentially unchanged from the case of two-point functions discussed earlier. The only difference is that we start the iterative process with a vacuum diagram in figure 4.4 instead of a two-point diagram in figure 2.7a.

Like in the SYK model, the contributions of N come from sums over free indices. When using the colouring convention of figure 4.3, every different colour gives a contribution of N since every colour corresponds to a free index. We note that from the graphical representation of the propagator shown in figure 4.1 it is clear that every line in a loop must have the same colour and we are free to choose this colour to be different for every loop. This means that a Feynman diagram with n index loops is proportional to N^n.

We can define a topological invariant, called Euler characteristic χ, for every graph in terms of the number of vertices v, edges (lines) e, and faces (areas enclosed within loops, including the exterior area outside the diagram) f. Then the Euler characteristic is defined as:

$$\chi = v - e + f. \tag{4.3.1}$$

The (black and white) graphs of this model have four lines (edges) coming out of every vertex. Because every line must be connected to two vertices, we can clearly express the number of edges is terms of the number of loops as $e = 2v$. Substituting this into the formula for the Euler characteristic and solving for the number of faces, we find that

$$f = \chi + v. \tag{4.3.2}$$

Let us now consider, as an example, the diagram of figure 4.4 and the fat subdiagram formed by removing the blue lines (figure 4.5b). By considering the double line formed by red and green lines as edges of a ribbon, we can form a ribbon diagram (see figure 4.7).

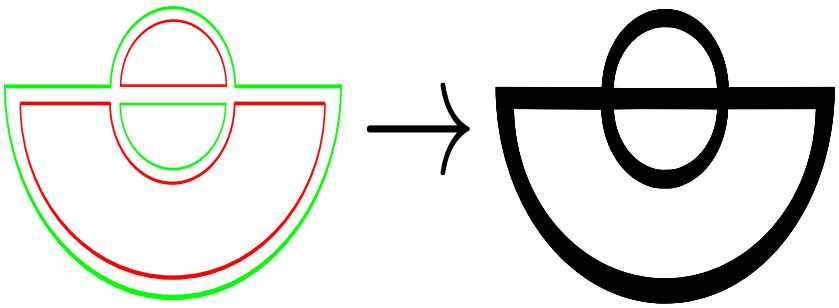

Figure 4.7: *By considering the red and green lines as edges of a ribbon, we can form a ribbon diagram.*

The Euler characteristic for the ribbon (a two-dimensional surface) can be analogously to the diagram case by setting $\chi = v - e + f$. Clearly for the ribbon diagram the previous conclusion that $f = \chi + v$ still holds. It is also easy to note that the number of faces of the ribbon diagram is exactly the number of loops in the red and green fat subdiagram i.e $n = f$. These conclusions are evidently general, so the number of index loops of the red and green fat subdiagram can be expressed as

$$n_{12} = \chi_{12} + v_{12}, \tag{4.3.3}$$

where n_{12} denotes the number of loops in a fat diagram with the green lines left out, χ_{12} the Euler characteristic of the corresponding ribbon diagram, and v_{12} the number of vertices of the fat diagram. On the other hand, we know that the loops in that fat subdiagram consist of all blue and red loops so that $n_{12} = f_1 + f_2$, where n_1 and n_2 denote the number of blue and red loops respectively. A similar result holds for the two other fat subdiagrams. Adding these all up and noting that the number of vertices is the same for all subdiagrams and equals that of the original diagram v, we get

$$n = n_1 + n_2 + n_3 = \frac{1}{2}(n_{01} + n_{12} + n_{02}) = \frac{1}{2}(\chi_{01} + \chi_{12} + \chi_{02} + 3v). \tag{4.3.4}$$

This can be expressed in terms of genus, $g = 1 - \frac{\chi}{2}$,

$$n = \frac{3}{2}v + 3 - (g_{01} + g_{12} + g_{02}). \tag{4.3.5}$$

It can be proven that the genus defined so is always (for the type of graph we are considering) a nonnegative, $0 \leq g$ [16]. Therefore we have the following inequality

for the number of index loops:

$$n \leq \frac{3}{2}v + 3. \tag{4.3.6}$$

Let us now show that the equality applies only for the iterated melonic diagrams. This will then establish the melonic dominance. Clearly this amounts to showing that $g_{01} = g_{12} = g_{02} = 0$ only for the fat subgraphs of iterated melonic diagrams.

Let us inspect the number of vertices each loop passes through. Denoting by $\mathcal{F}_m$ the number of loops that pass through m vertices. Since there are no tadpole diagrams, so that $\mathcal{F}_1 = 0$, we can express the total number of index loops as

$$n = \frac{3}{2}v + 3 = \sum_{m=2}^{\infty} \mathcal{F}_m. \tag{4.3.7}$$

On the other hand, we know that since there are two incoming and two outgoing lines of each colour in each vertex, every vertex must be passed 6 times. Therefore we get a following expression for v:

$$6v = \sum_{m=2}^{\infty} m\mathcal{F}_m. \tag{4.3.8}$$

Substituting (4.3.8) to earlier result (4.3.7) and rearranging, we find that

$$2\mathcal{F}_2 + \mathcal{F}_3 = 12 + \sum_{m=5}^{\infty} (m-4)\mathcal{F}_m. \tag{4.3.9}$$

Let us now show that a graph with $g = 0$ must necessarily have $\mathcal{F}_3 = 0$. It is easiest to use the result from graph theory that a genus of a graph is 0 if and only if it is a planar graph [18]. Therefore we need only to show that graph that has a loop passing three vertices cannot be planar. The index loop passing three vertices is of the form shown in the figure 4.8a, up to the choice of the colour of the line, which does not matter, since the three different ways of representing vertices (figure 4.2) are equivalent, so using a different colour amounts to choosing a different way of representing the vertex.

To complete the diagram, we must add the lines of the two remaining colours so that each vertex is of the form (4.2)a. Without loss of generality we may choose

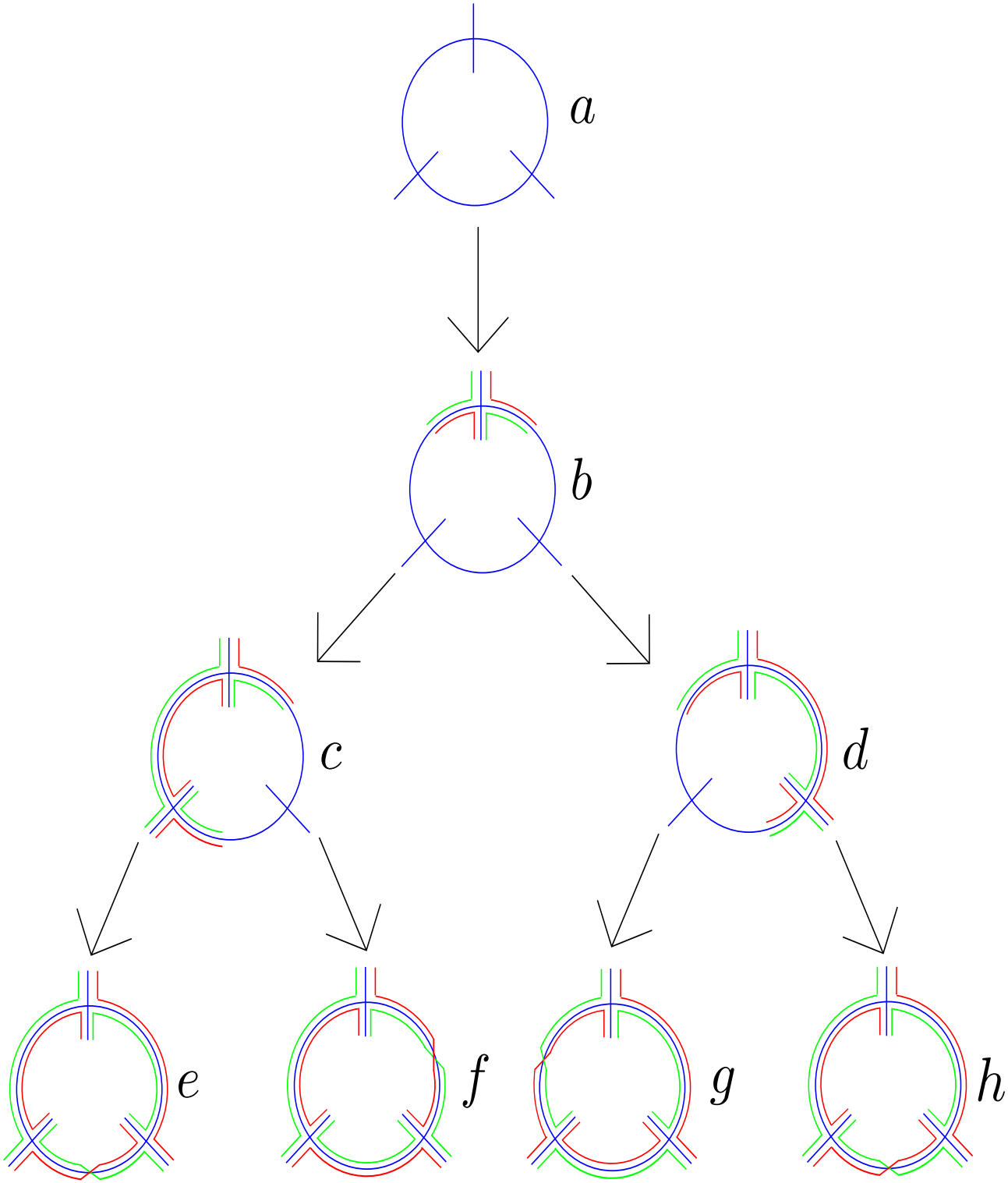

Figure 4.8: *All the possible colourings of an index loop with three vertices. Note that we have not explicitly drawn the rest of the diagram as a black box as usual, but this is assumed implicitly.*

Starting from the general type of an index loop with three vertices (a), we can, without loss of generality, first colour one vertex to get the diagram (b). To keep the graph planar, we can move either one vertex clockwise (d) or anti-clockwise (c) and colour that vertex so that the resulting diagram is planar. In both cases, we notice that the only possible colourings for the final vertex in cases (e,f,g,h) will result in a non-planar graph.

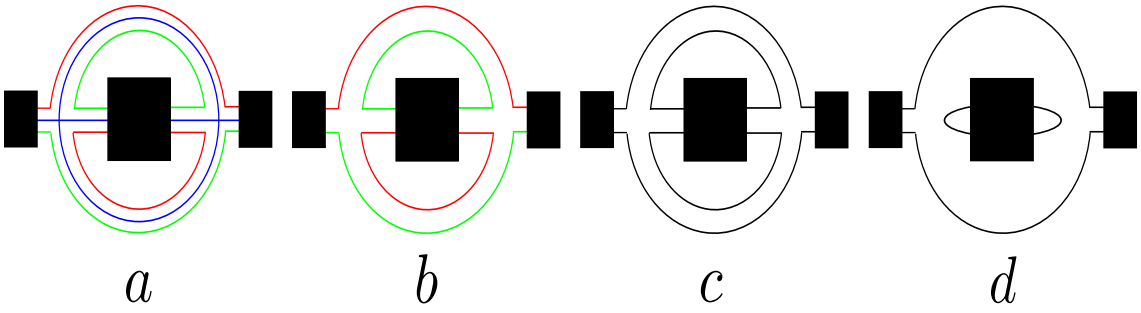

Figure 4.9: *Index loop with two vertices. The figure (a) shows the most general index loop passing through two vertices. In (b) we have left the blue lines out, getting a diagram of familiar type from matrix models. We can then uncolour the lines (c) so that we can connect red and green lines without the risk of confusion. Then we can divide the diagram into two separate genus zero parts (d).*

one vertex and add green and red lines. Then we get a diagram in figure 4.8b up to exchanging green and red colours with each other. Then if we want to keep the diagram planar, we must add the coloured lines to the next vertex either in the way shown in the figure 4.8c or 4.8d. In either case, we have two more choices for colouring the last vertex. As can be seen from the figure 4.8e,f,g,h, all of them lead to a non-planar diagram, which in turn implies $g \neq 0$. Therefore we deduce that for diagrams with $g = 0$, we must have $\mathcal{F}_3 = 0$. As a side note, it is easy to see that similar argument shows that any diagram with $\mathcal{F}_m = 0$ for odd m is non-planar.

Since for graphs of genus 0 $\mathcal{F}_3 = 0$, and all the terms on the right-hand side of the relation (4.3.9) are positive, we must have $\mathcal{F}_2 > 0$ for graphs with $g = 0$. Let us now show that any graph with $\mathcal{F}_2 > 0$ and $g = 0$ is necessarily an iterated melonic diagram. The only index loop passing two vertices is (up to the choice of colours) shown in the figure 4.9a.

The fat subgraph without blue lines is shown in (4.9)b. Let us now modify this graph by first uncolouring the lines (so that we may attach a red line to a green line). Then we can cut the graph in the middle off the index loop passing through two vertices as shown in the figure 4.9c. Then we can attach the external lines of the inner graph to each other and do the same for the two new external lines of the

index loop (see figure 4.9). These operations do not change the amount of vertices or loops but remove two edges, so $f_{new} = f_{old}$, $e_{new} = e_{old} - 2$ and $v_{new} = v_{old}$. By assumption $g = 0$ for the original diagram, so $\chi_{old} = 2 - 2g = 2$. By the definition of the Euler characteristic

$$\chi_{new} = f_{new} - e_{new} + v_{new} = f_{old} - e_{old} + v_{old} + 2 = \chi_{old} + 2 = 4. \tag{4.3.10}$$

On the other hand the Euler characteristic of two distinct diagrams is the sum of the Euler characteristics of the two diagrams:

$$4 = \chi_{new} = \chi_1 + \chi_2 = 4 - 2(g_1 + g_2). \tag{4.3.11}$$

But we know that $g_1, g_2 \geq 0$, so we must have that $g_1 = g_2 = 0$. We now have two possibilities: either the black boxes represent trivial diagrams so that the diagram of figure 4.9 is itself a melonic diagram or then one or more of the black boxes are non-trivial. However, since both diagrams have $g = 0$, the argument above applies for them, and we can cut them into two genus zero parts. We can then continue this process until we arrive to point where all black boxes represent trivial diagrams, and we have divided the diagram into melons. Then we deduce that the diagram must be an iterated melonic diagram. This finishes the proof.

4.4 Two-point Function

We have shown that in the case of vacuum diagrams only the melonic diagrams contribute in the leading order. The proof is completely similar in the case of the two-point functions, since we can "cut" one line in the vacuum diagram to get a diagram for the two-point function. It is clear that this does not affect the proof presented in the previous section.

Because only melonic diagrams contribute to the two-point function, we again get (apart from the constant prefactors) the same Schwinger-Dyson equation (2.4.4) as for the original SYK model (see figure 2.10c):

$$G(0,t) = -\frac{1}{2}\mathrm{sgn}(t) - J^2N^3 \int dt_1 dt_2 \frac{1}{2}\mathrm{sgn}(t_1)G(t_1,t_2)^3 G(t_2,t). \tag{4.4.1}$$

In the infrared limit this has the same solution as before, apart from the prefactors.

$$G(t_1, t_2) = -\left(\frac{1}{4\pi g^2 N^3}\right)^{1/4} \frac{\mathrm{sgn}(t_1 - t_2)}{\sqrt{|t_1 - t_2|}}. \tag{4.4.2}$$

4.5 Four-point Function

For the SYK-like model discussed in this section, the four-point function is given by the following product

$$\langle \psi^{a_1 a_2 a_3}(t_1) \psi^{a_1 b_2 b_3}(t_2) \psi^{c_1 a_2 b_3}(t_3) \psi^{c_1 b_2 a_3}(t_4) \rangle. \tag{4.5.1}$$

Note that unlike when calculating the four-point function for the SYK model, here we do not have to average over different field configurations.

With obvious modifications to the proof in the section 4.3, it is easy to show that the leading-order corrections are again given by the iterated ladder diagrams (see figure 2.13). In particular we have that

$$\langle \psi^{a_1 a_2 a_3}(t_1) \psi^{a_1 b_2 b_3}(t_2) \psi^{c_1 a_2 b_3}(t_3) \psi^{c_1 b_2 a_3}(t_4) \rangle = N^6 G(t_1, t_2) G(t_3, t_4) + \Gamma(t_1, t_2, t_3, t_4) \tag{4.5.2}$$

with the n-rung ladder diagrams satisfying again the recursion relation:

$$\Gamma_{n+1} = \int dt_a dt_b K(t_1, t_2, t_a, t_b) \Gamma_n(t_a, t_b, t_3, t_4). \tag{4.5.3}$$

The only differences are the definition of Γ_0:

$$\Gamma_0(t_1, t_2, t_3, t_4) = N^3(-G(t_1, t_3)G(t_2, t_4) + G(t_1, t_4)G(t_2, t_3)), \tag{4.5.4}$$

which differs by the prefactor of $N^{3/2}$ from the SYK result (remember that the two-point functions $G(t, t')$ are proportional to $N^{-3/4}$). The other difference is in the definition of the kernel:

$$K(t_1, t_2, t_3, t_4) = -3J^2 N^3 G(t_1, t_3) G(t_2, t_4) G(t_3, t_4)^2. \tag{4.5.5}$$

Here the powers of N cancel so we see that the kernel is actually exactly the same as for the SYK model.

Due to the kernel (and the two-point functions) having exactly the same functional form as those of the SYK model, we immediately deduce that the eigenfunctions of the kernel are given by (2.5.59):

$$F_\alpha(\chi) = \begin{cases} \frac{\Gamma(2\alpha)^2}{2\Gamma(4\alpha)}(1+\sec(2\pi\alpha))\chi^{2\alpha}{}_2F_1(2\alpha,2\alpha,4\alpha,\chi) & \\ -\frac{\Gamma(1-2\alpha)^2}{2\Gamma(2-4\alpha)}\tan(2\pi\alpha)\tan(\pi\alpha)\chi^{1-2\alpha}{}_2F_1(1-2\alpha,1-2\alpha,2-4\alpha,\chi) & 0<\chi<1 \\ \frac{\Gamma\left(\frac{1}{2}-\alpha\right)\Gamma(\alpha)}{\sqrt{\pi}}{}_1F_2\left(\alpha,\frac{1}{2}-\alpha,\frac{1}{2},\frac{(2-\chi)^2}{\chi^2}\right) & 1<\chi \end{cases} \tag{4.5.6}$$

and have eigenvalues given by (2.5.80).

$$g(\alpha) = \frac{3}{4\alpha-1}\tan\left(\pi\left(\frac{1}{4}-\alpha\right)\right), \tag{4.5.7}$$

where $\alpha = 1/4 + is$ with $s \in \mathbb{R}$ or $\alpha = n$ with $n \in \mathbb{N}$.

Also the diagonalisation of the kernel proceeds in the same way as before, giving us the following result for the four-point function:

$$\begin{aligned}\Gamma(t_1,t_2,t_3,t_4) &= \frac{8N^3}{\pi}G(t_1,t_2)G(t_3,t_4)\int_0^\infty ds\frac{\tanh(2\pi s)}{4s\coth(\pi s)-3}F_{1/4+is}(\chi) \\ &+N^3G(t_1,t_2)G(t_3,t_4)\sum_{n\neq 2}\left(\frac{(1-4n)^2\cot(2\pi n)}{\pi^2\left(4n-3\cot\left(\pi\left(n+\frac{1}{4}\right)\right)-1\right)}-\frac{2\pi}{3}\right)F_n(\chi)+\delta\Gamma,\end{aligned} \tag{4.5.8}$$

where $\delta\Gamma$ again denotes the contribution of the divergent term with eigenvalue $g(1) = 1$. In the perturbative theory, the leading-order correction is given by

$$\begin{aligned}\delta\Gamma(\theta_1,\theta_2,\theta_3,\theta_4) &= N^3G(\theta_1,\theta_2)G(\theta_3,\theta_4)\,\frac{3\sqrt{2}}{2\pi+3\pi^2}\,\beta J\sum_{|n|\geq 2}\frac{e^{in/2(\theta_1+\theta_2+\theta_3+\theta_4)}}{n^2(n^2-1)} \\ &\times\left(\frac{\sin\left(n\frac{\theta_1-\theta_2}{2}\right)}{\tan\left(\frac{\theta_1-\theta_2}{2}\right)}-n\cos\left(n\frac{\theta_1-\theta_2}{2}\right)\right)\left(\frac{\sin\left(n\frac{\theta_3-\theta_4}{2}\right)}{\tan\left(\frac{\theta_3-\theta_4}{2}\right)}-n\cos\left(n\frac{\theta_3-\theta_4}{2}\right)\right),\end{aligned} \tag{4.5.9}$$

where this expression is again understood to be evaluated on the thermal circle, which corresponds to a transformation

$$t_i = \tan\left(\frac{\theta_i}{2}\right). \tag{4.5.10}$$

If the conjecture in [14] is correct and the change in eigenvalues to the second order in $1/(\beta J)$ is given by

$$g(1,n) = 1 - \frac{4g'(2)k}{\beta J}|n| 8g''(2)\left(\frac{k|n|}{\beta J}\right)^2 + O(1/(\beta J)^3), \tag{4.5.11}$$

we find that the tensor model has a four-point function, up to order $1/(\beta J)^0$ given by:

$$\begin{aligned}\delta\Gamma(\theta_1,\theta_2,\theta_3,\theta_4) = N^3 G(x)G(x')\Bigg(&\frac{1}{\sqrt{2}}\beta J - 2(y-y'-\pi/2)\partial_{y-y'} + 2(x-\pi)\delta_x \\ &+ 2(x'-\pi)\delta_{x'}\Bigg)\sum_{|n|\geq 2}\frac{e^{in(y-y')}}{\pi^2 n^2(n^2-1)}\left(\frac{\sin\left(n\frac{x}{2}\right)}{\tan\left(\frac{x}{2}\right)} - n\cos\left(n\frac{x}{2}\right)\right) \\ &\times\left(\frac{\sin\left(n\frac{x'}{2}\right)}{\tan\left(\frac{x'}{2}\right)} - n\cos\left(n\frac{x'}{2}\right)\right),\end{aligned} \tag{4.5.12}$$

where

$$x = \theta_1 - \theta_2, \qquad x' = \theta_3 - \theta_4, \qquad y = \frac{\theta_1-\theta_2}{2}, \qquad y' = \frac{\theta_3-\theta_4}{2}. \tag{4.5.13}$$

5. Chaotic Behaviour

5.1 Chaotic Behaviour in Quantum Systems

Thus far, we have mostly inspected the SYK model in the zero temperature, or in the $\beta \to \infty$ limit. It is, however, useful to inspect the properties of the model also in finite temperatures. One property that we can then investigate is the chaotic behaviour of the system. We have to bear in mind, however, that many of the properties of the two- and four-point functions we derived in the previous chapters depend on the conformal symmetry of the two-point function, which is exact only in the low-energy limit.

The chaotic behaviour of a general quantum system can be characterised using a time-separated commutator $[W(t), V(0)]$ between two Hermitian operators $W(t)$ and $V(t)$. Roughly speaking, this commutator measures the effect of a perturbation by $V(0)$ on the measurements of $W(t)$ at a later time t and vice versa. One possible measure of the chaotic behaviour of the system is then [5]:

$$C(t) = \langle [W(t), V(0)]^2 \rangle = Z^{-1} \mathrm{Tr} \left[e^{-\beta H} [W(t), V(0)]^2 \right], \tag{5.1.1}$$

where $\beta = T^{-1}$ and $Z = \mathrm{Tr}[e^{-\beta H}]$ as usual. We say that the system exhibits chaotic behaviour if

$$C(t) \sim 2\langle W(t)W(t)\rangle\langle V(0)V(0)\rangle \tag{5.1.2}$$

for large values of $C(t)$, regardless of specific forms of operators $W(t)$ and $V(t)$. The only restriction is that they are both Hermitian operators that can be described as

a sum of terms that have only $O(1)$ degrees of freedom and that the operators have zero thermal one-point functions. [5]

To see that the squared commutator $C(t)$ indeed has a connection to the chaotic behaviour, we can consider the case $W(t) = q(t)$ $V(t) = p(t)$, for simplicity in one spatial dimension, in the semiclassical limit [19, 20, 5]. In this limit, the commutator $[W(t), V(0)]$ becomes a Poisson bracket, so we have that

$$[W(t), V(0)] \to i\hbar\{q(t), p(0)\} = i\hbar\frac{\partial q(t)}{\partial q(0)}. \tag{5.1.3}$$

Therefore we see that the commutator describes how the position of the system depends on its original position or how the nearby trajectories of the system diverge. Classically such divergence is quantified by the Lyapunov exponent λ_L, which can be defined through the relation

$$|\delta\mathbf{q}(t)| = e^{\lambda_L t}|\delta\mathbf{q}(0)| \tag{5.1.4}$$

in the linear approximation, where $\delta\mathbf{q}(t)$ denotes the change of the position of the system at time t. Going to one spatial dimension and taking limit $|\delta\mathbf{q}(0)| \to 0$, we get that

$$\lim_{|\delta\mathbf{q}(0)|\to 0}\frac{|\delta\mathbf{q}(t)|}{|\delta\mathbf{q}(0)|} = \lim_{\delta q(0)\to 0}\frac{\delta q(t)}{\delta q(0)} = \frac{\partial q(t)}{\partial q(0)} = e^{\lambda_L t}. \tag{5.1.5}$$

Combining expressions (5.1.3) and (5.1.5) we see that the commutator $[W(t), V(0)]$ has indeed a direct connection with chaotic behaviour, at least in the semi-classical limit.

While (5.1.1) is a perfectly valid measure of chaotic behaviour for example for lattice systems, it usually diverges in the thermal field theories, so it needs to be regularized. One option is to study instead the following function, which corresponds to moving the other commutator halfway around the thermal circle:

$$C(t) = -\mathrm{Tr}\left[y^2[W(t), V(0)]y^2[W(t), V(0)]\right], \tag{5.1.6}$$

where y is defined by

$$y = \frac{1}{Z^{1/4}}e^{-\frac{\beta}{4}H}. \tag{5.1.7}$$

To "separate the chaotic behaviour", it is useful to define the following quantity $F(t)$, which intuitively corresponds to a situation where the operators $W(t)$ and $V(0)$ are placed alternatingly on the thermal circle with equal intervals:

$$F(t) = \mathrm{Tr}[yV(0)yW(t)yV(0)yW(t)]. \tag{5.1.8}$$

We can then use complex time argument for $F(t)$ to get another form for this function.

$$\begin{aligned}
&F(t+i\beta/4) = \mathrm{Tr}[yV(0)yW(t+i\beta/4)yV(0)yW(t+i\beta/4)] \\
&= \mathrm{Tr}\left[\frac{1}{Z}e^{-\frac{\beta}{4}H}V(0)e^{-\frac{\beta}{4}H}W(t+i\beta/4)e^{-\frac{\beta}{4}H}V(0)e^{-\frac{\beta}{4}H}W(t+i\beta/4)\right] \\
&= \mathrm{Tr}\left[\frac{1}{Z}e^{-\frac{\beta}{4}H}V(0)e^{-\frac{\beta}{4}H}e^{-iH\left(i\frac{\beta}{4}\right)}W(t)e^{iH\left(i\frac{\beta}{4}\right)}e^{-\frac{\beta}{4}H}V(0)e^{-\frac{\beta}{4}H}e^{-iH\left(i\frac{\beta}{4}\right)}W(t)e^{iH\left(i\frac{\beta}{4}\right)}\right] \\
&= \mathrm{Tr}\left[yV(0)W(t)y^2V(0)W(t)\right] \\
&= \mathrm{Tr}\left[y^2V(0)W(t)y^2V(0)W(t)\right].
\end{aligned} \tag{5.1.9}$$

Then using (5.1.9) and similar result for $F(t-i\beta/4)$, we get a following expression

$$\begin{aligned}
&C(t) = -\mathrm{Tr}\left[y^2[W(t),V(0)]y^2[W(t),V(0)]\right] = \mathrm{Tr}[y^2W(t)V(0)y^2V(0)W(t)] \\
&+ \mathrm{Tr}[y^2V(0)W(t)y^2W(t)V(0)] - F(t-i\beta/4) - F(t+i\beta/4).
\end{aligned} \tag{5.1.10}$$

To show that the first two terms are of order one regardless of the time t, we can represent them as inner products of thermal field double states. Let us define the thermal field double state $|TDF\rangle$ as

$$|TFD\rangle = \frac{1}{Z^{1/2}}\sum_n e^{-\frac{\beta}{2}E_n}|n\rangle_L|n\rangle_R. \tag{5.1.11}$$

Let us, furthermore, denote the operators $I\oplus W(t) = W_R(t)$, $W(t)\oplus I = W_L(t)$ and similarly for the other operators. Then we can write the first term on the right-hand

side of (5.1.10) as

$$\begin{aligned}
&\mathrm{Tr}[y^2W(t)V(0)y^2V(0)W(t)] \\
&= \mathrm{Tr}[yW(t)V(0)y^2V(0)W(t)y] \\
&= \sum_n \langle n|yW_R(t)V_R(0)y^2W_R(t)V_R(0)y|n\rangle \\
&= \sum_{n,m} \langle m|n\rangle_L \, \langle m|e^{-\frac{\beta}{2}E_n}y^{-1}W_R(t)V_R(0)y^2W_R(t)V_R(0)y^{-1}e^{-\frac{\beta}{2}E_n}|n\rangle_R \\
&= \langle TFD|y^{-1}W_R(t)V_R(0)y^2W_R(t)V_R(0)y^{-1}|TFD\rangle \\
&= |yV_R(0)W_R(t)y^{-1}\,|TFD\rangle\,|^2. \qquad (5.1.12)
\end{aligned}$$

We have a similar expansion for the second term on the right-hand side of (5.1.10). Therefore the first two terms are of the order one for arbitrary time t. The same argument cannot be used for the last two terms $F(t\pm i\beta/4)$ since the operators $V(0)$ and $W(t)$ are in an alternating order in these terms. We could, however, express them in terms of a perturbed state $|\Psi\rangle$:

$$|\Psi(t)\rangle = \frac{1}{Z^{1/2}}\sum_{n,m} e^{-\frac{\beta}{4}\beta(E_n+E_m)}W(t)_{nm}\,|m\rangle_L\,|n\rangle_R\,. \qquad (5.1.13)$$

Then we would have

$$F(t\pm i\beta/4) = \langle\Psi(t\pm i\beta/4)|V_LV_R|\Psi(t\pm i\beta/4)\rangle\,. \qquad (5.1.14)$$

This, however, is not a norm, so there is no requirement for this to be of order one. Indeed, we see that in order to have $C(t)\sim 2\langle W(t)W(t)\rangle\langle V(0)V(0)\rangle$, which was our previous definition of chaotic behaviour, we need the functions $F(t\pm i\beta/4)$ become small in order for $C(t)$ grow. Thus we can define a chaotic system as one where $F(t)\to 0$ as $t\to\infty$.

Using (5.1.13) and (5.1.14), we can also interpret $F(t)$ as a correlation function in terms of a $|\Psi(t)\rangle$, which can be viewed as $|TFD\rangle$ perturbed by $W(t)$. [5] For small values of t, the assumption of simpleness of $W(t)$ guarantees that the perturbation does not have a significant effect, so the correlation function $F(t)$ remains large. For large values of t, $W(t)$ has a sizeable effect, which disrupts the thermal field double state and the correlation becomes small [6].

5.2 Lyapunov Exponent for the SYK Model

To find the maximal Lyapunov exponent for the SYK model, we need to consider it in finite nonzero temperature instead of zero temperature ($\beta \to \infty$) limit we have been considering so far. To do this, we can go back to the low-energy solution (2.4.26):

$$G(t_1, t_2) = -\left(\frac{1}{4\pi J^2}\right)^{1/4} \frac{1}{\sqrt{|t_1 - t_2|}} \mathrm{sgn}(t_1 - t_2). \tag{5.2.1}$$

We can without loss of generality again set $t_1 = t$ $t_2 = 0$ by the time translation invariance. Recalling the reparametrization invariance (2.4.12):

$$G(s, s') = \left|\frac{df(s)}{ds}(s)\right|^{1/4} \left|\frac{df(s)}{ds}(s')\right|^{1/4} G(f(s), f(s')). \tag{5.2.2}$$

we can the set $f(t) = \tan\left(\frac{\pi t}{\beta}\right)$, which maps the value $\beta \to \infty$ to a finite value and gives us the finite temperature two-point function:

$$G(t, 0) = -\left(\frac{1}{4\pi J^2}\right)^{1/4} \sqrt{\frac{\pi}{\beta \left|\sin\left(\frac{\pi t}{\beta}\right)\right|}} \mathrm{sgn}(t). \tag{5.2.3}$$

We can compute the two-point function also in the Lorentzian time by analytically continuing this solution to $t = i\tau$, where τ is the Lorentzian time opposed to the Euclidean time t we have been using so far. Since the two-point function (5.2.3) has a divergence at $t = 0$, we can continue the function either in the $t > 0$ or $t < 0$ regime. Analytic continuation to Lorentzian time in the $t > 0$ case gives

$$\begin{aligned}\langle \chi(\tau)\chi(0)\rangle = G_L(\epsilon + i\tau) &= -\left(\frac{1}{4\pi J^2}\right)^{1/4} \sqrt{\frac{\pi}{\beta \sin\left(\frac{\pi i\tau}{\beta}\right)}} \\ &= -\left(\frac{1}{4\pi J^2}\right)^{1/4} \sqrt{\frac{\pi}{i\beta \sinh\left(\frac{\pi\tau}{\beta}\right)}} = -\left(\frac{1}{4\pi J^2}\right)^{1/4} e^{-i\pi/4} \sqrt{\frac{\pi}{\beta \sinh\left(\frac{\pi\tau}{\beta}\right)}},\end{aligned} \tag{5.2.4}$$

where we have denoted the analytical continuation in the $t > 0$ regime by $G_L(\epsilon + i\tau)$. Similarly, the analytic continuation in the $t < 0$ case gives:

$$\begin{aligned}\langle \chi(0)\chi(\tau)\rangle = G_L(-\epsilon + i\tau) &= -\left(\frac{1}{4\pi J^2}\right)^{1/4} \sqrt{\frac{\pi}{-\beta \sin\left(\frac{\pi i\tau}{\beta}\right)}} \\ &= -\left(\frac{1}{4\pi J^2}\right)^{1/4} e^{i\pi/4} \sqrt{\frac{\pi}{i\beta \sinh\left(\frac{\pi\tau}{\beta}\right)}}.\end{aligned} \tag{5.2.5}$$

We can then define the retarded propagator as

$$G_R(\tau) = \langle \chi(\tau)\chi(0) + \chi(0)\chi(\tau)\rangle\theta(\tau) = (G_L(\epsilon + i\tau) + G_L(-\epsilon + i\tau))\theta(\tau)$$
$$= \left(\frac{\pi}{J^2}\right)^{1/4} \frac{1}{\sqrt{\beta \sinh\left(\frac{\pi\tau}{\beta}\right)}}\theta(\tau). \tag{5.2.6}$$

As discussed previously, to probe the chaotic behaviour of the SYK model we can calculate the following function:

$$F(\tau_1, \tau_2) = \mathrm{Tr}[y\chi_i(\tau_1)y\chi_j(0)y\chi_i(\tau_2)y\chi_j(0)]. \tag{5.2.7}$$

It can be shown [14] that the solution is given again by ladder diagrams, but which this time are on the time contour that covers the thermal circle and has two real-time folds that correspond to times τ_1 and τ_2. To find the growth exponent or the Lyapunov exponent, it is sufficient to consider the asymptotic growth of $F(\tau_1, \tau_2)$. The asymptotic leading-order correction depends only on the value of $F(\tau_1, \tau_2)$ on the real-time part of the contour [14]. It is useful to define the retarder kernel for the ladder diagrams by

$$K_R(\tau_1, \tau_2, \tau_3, \tau_4) = 3J^2 G_R(\tau_1 - \tau_3)G_R(\tau_2 - \tau_4)G_{lr}(\tau_3 - \tau_4)^2, \tag{5.2.8}$$

where $G_{lr}(\tau)$ denotes the Wightman correlator, where the two fields are separated by a quarter of the thermal circle in addition to the real time separation:

$$G_{lr}(\tau) = \langle \chi(i\tau + \pi\beta/2)\chi(0)\rangle = \left(\frac{\pi}{4J^2}\right)^{1/4} \frac{1}{\sqrt{\beta \cosh\left(\frac{\pi\tau}{\beta}\right)}}. \tag{5.2.9}$$

The asymptotic growth of $F(\tau_1, \tau_2)$ is determined by a condition that adding another rung to the ladder $F(\tau_1, \tau_2)$ will not affect the value of the ladder. In other words $F(\tau_3, \tau_4)$ must be an eigenvector of the retarder kernel $K_R(\tau_1, \tau_2, \tau_3, \tau_4)$ with an eigenvalue of 1, so it must satisfy the following integral equation:

$$F(\tau_1, \tau_2) = \int d\tau_3 d\tau_4 K_R(\tau_1, \tau_2, \tau_3, \tau_4)F(\tau_3, \tau_4). \tag{5.2.10}$$

On the basis of previous discussion, we expect that the four-point function $F(\tau_1, \tau_2)$ should be proportional to $e^{\lambda_L(\tau_1+\tau_2)/2}$, so that setting $\tau_1 = \tau_2 = \tau$ gives that

$$F(\tau, \tau) = \mathrm{Tr}[y\chi_i(\tau)y\chi_j(0)y\chi_i(\tau)y\chi_j(0)] \sim e^{\lambda_L \tau}, \tag{5.2.11}$$

as it should be by the previous discussion. Therefore we can use a trial function of the form

$$F(\tau_3, \tau_4) = e^{\lambda_L(\tau_3+\tau_4)/2} f(\tau_3 - \tau_4). \tag{5.2.12}$$

Substituting this to the integral equation (5.2.10), using the definition of the retarded kernel (5.2.8) and the definitions of the retarded propagator (5.2.6) and the Wightman propagator (5.2.9), we get a following integral equation:

$$F(\tau_1, \tau_2) = 3J^2 \int d\tau_3 d\tau_4 \frac{\pi}{\sqrt{2}J^2\beta^2} \frac{1}{\sqrt{\sinh\left(\frac{\pi(\tau_1-\tau_3)}{\beta}\right)}} \frac{1}{\sqrt{\sinh\left(\frac{\pi(\tau_2-\tau_4)}{\beta}\right)}} \frac{1}{\cosh\left(\frac{\pi(\tau_3-\tau_4)}{\beta}\right)}$$
$$\times e^{\lambda_L(\tau_3+\tau_4)/2} f(\tau_3 - \tau_4). \tag{5.2.13}$$

Relatively straightforward integration, similar to those performed earlier, shows that a function $f(\tau_3 - \tau_4)$ satisfying this equation is given by [14]:

$$f(\tau_3 - \tau_4) = \frac{1}{\cosh\left(\frac{\pi}{\beta}(\tau_3 - \tau_4)\right)^{3/2}}. \tag{5.2.14}$$

This is enough to show that the growth rate of $F(\tau, \tau)$ is proportional to $2\pi/\beta$, so we can identify the Lyapunov exponent as

$$\lambda_L = \frac{2\pi}{\beta}. \tag{5.2.15}$$

It can be shown [5] that for a large class of quantum theories, including large N theories, this is the maximal allowed Lyapunov exponent. Interestingly, it can be shown that a black hole in Einstein gravity also has the same Lyapunov exponent [6]. This is one piece of evidence that lead Kitaev to propose the SYK model as a holographic dual for a Schwarzschild black hole in $1+1$ dimensional, asymptotically AdS, spacetime [2].

Bibliography

[1] Subir Sachdev and Jinwu Ye. "Gapless spin fluid ground state in a random, quantum Heisenberg magnet". In: *Phys. Rev. Lett.* 70 (1993), p. 3339. DOI: 10.1103/PhysRevLett.70.3339. arXiv: cond-mat/9212030 [cond-mat].

[2] A. Kitaev. *A Simple Model Of Quantum Holography*. 2015. URL: http://online.kitp.ucsb.edu/online/entangled15/kitaev/.

[3] Joseph Polchinski and Vladimir Rosenhaus. "The Spectrum in the Sachdev-Ye-Kitaev Model". In: *JHEP* 04 (2016), p. 001. DOI: 10.1007/JHEP04(2016)001. arXiv: 1601.06768 [hep-th].

[4] Subir Sachdev. "Holographic metals and the fractionalized Fermi liquid". In: *Phys. Rev. Lett.* 105 (2010), p. 151602. DOI: 10.1103/PhysRevLett.105.151602. arXiv: 1006.3794 [hep-th].

[5] Juan Maldacena, Stephen H. Shenker, and Douglas Stanford. "A bound on chaos". In: *JHEP* 08 (2016), p. 106. DOI: 10.1007/JHEP08(2016)106. arXiv: 1503.01409 [hep-th].

[6] Stephen H. Shenker and Douglas Stanford. "Black holes and the butterfly effect". In: *JHEP* 03 (2014), p. 067. DOI: 10.1007/JHEP03(2014)067. arXiv: 1306.0622 [hep-th].

[7] Juan Martin Maldacena. "The Large N limit of superconformal field theories and supergravity". In: *Int. J. Theor. Phys.* 38 (1999). [Adv. Theor. Math. Phys.2,231(1998)], pp. 1113–1133. DOI: 10.1023/A:1026654312961. arXiv: hep-th/9711200 [hep-th].

[8] Makoto Natsuume. *AdS/CFT Duality User Guide*. 2016. ISBN: 9784431554417. arXiv: arXiv:1409.3575v4.

[9] Edward Witten. "An SYK-Like Model Without Disorder". In: (2016). arXiv: 1610.09758 [hep-th].

[10] Razvan Gurau. "Colored Group Field Theory". In: *Commun. Math. Phys.* 304 (2011), pp. 69–93. DOI: 10.1007/s00220-011-1226-9. arXiv: 0907.2582 [hep-th].

[11] Razvan Gurau and Vincent Rivasseau. "The 1/N expansion of colored tensor models in arbitrary dimension". In: *Europhys. Lett.* 95 (2011), p. 50004. DOI: 10.1209/0295-5075/95/50004. arXiv: 1101.4182 [gr-qc].

[12] Razvan Gurau. "The complete 1/N expansion of colored tensor models in arbitrary dimension". In: *Annales Henri Poincare* 13 (2012), pp. 399–423. DOI: 10.1007/s00023-011-0118-z. arXiv: 1102.5759 [gr-qc].

[13] Michael E. Peskin and Daniel V. Schroeder. *Introduction to Quantum Field Theory*. Reading, Massachusetts: Perseus Books, 1995.

[14] Juan Maldacena and Douglas Stanford. "Remarks on the Sachdev-Ye-Kitaev model". In: *Phys. Rev.* D94.10 (2016), p. 106002. DOI: 10.1103/PhysRevD.94.106002. arXiv: 1604.07818 [hep-th].

[15] David J. Gross and Vladimir Rosenhaus. "A Generalization of Sachdev-Ye-Kitaev". In: *JHEP* 02 (2017), p. 093. DOI: 10.1007/JHEP02(2017)093. arXiv: 1610.01569 [hep-th].

[16] Igor R. Klebanov and Grigory Tarnopolsky. "Uncolored random tensors, melon diagrams, and the Sachdev-Ye-Kitaev models". In: *Phys. Rev.* D95.4 (2017), p. 046004. DOI: 10.1103/PhysRevD.95.046004. arXiv: 1611.08915 [hep-th].

[17] Sylvain Carrozza and Adrian Tanasa. "$O(N)$ Random Tensor Models". In: *Lett. Math. Phys.* 106.11 (2016), pp. 1531–1559. DOI: 10.1007/s11005-016-0879-x. arXiv: 1512.06718 [math-ph].

[18] Richard J. Trudeau. *Introduction to Graph Theory*. New York: Dover Publications, 1993.

[19] A. Kitaev. *Hidden Correlations in the Hawking Radiation and Thermal Noise*. 2015. URL: http://online.kitp.ucsb.edu/online/joint98/kitaev/.

[20] A. I. Larkin and Yu. N. Ovchinnikov. "Quasiclassical Method in the Theory of Superconductivity". In: *JETP* 28.6 (1969), pp. 1200–1205.